

Validation of a simulation model for
stick-slip prediction
Dct 2004.67

M.J. Nieuwenhuizen

Supervisors:
prof.dr.ir. M. Steinbuch
ir. P.W.J.M. Nuij
ir. R.v. Rijswijk

TU/e
TU/e
Rexroth Hydraudyne

CONTENTS

NOMENCLATURE.....	3
INTRODUCTION.....	5
CHAPTER 1 LOCK MODEL	7
1.1 DESCRIPTION OF THE SYSTEM	7
1.2 MODEL OF THE LOCK	9
1.2.1 Model of the cylinder.....	9
1.2.2 Model of the hydraulic system.....	10
1.2.3 Model of the driven system.....	11
CHAPTER 2 MEASUREMENT SETUP FOR IDENTIFICATION OF THE PARAMETERS.....	14
CHAPTER 3 MEASUREMENTS ON THE LOCK.....	15
3.1 MEASUREMENT EQUIPMENT AND PLACEMENT.....	15
3.2 DATA ACQUISITION.....	16
3.3 MEASUREMENTS.....	17
CHAPTER 4 PRE-PROCESSING THE DATA.....	18
4.1 TOOLS FOR SIGNAL ANALYSIS	18
4.2 PRE-PROCESSING THE DATA	19
4.2.1 The velocity measurements.....	19
4.2.2 The displacement measurement with the laser vibrometer.....	20
4.2.3 Displacement measurement with the CIMS.....	20
4.2.4 The acceleration measurements	21
4.2.5 The strain gauge signal	22
4.2.6 Pressure signals.....	23
CHAPTER 5: RESULTS AND IDENTIFICATION.....	23
5.1 FREQUENCY ANALYSIS	25
5.2 IDENTIFICATION OF THE HYDRAULIC SYSTEM.....	25
5.2.1 Calculating the pressure time derivative.....	26
5.2.2 Calculating R_i from the stationary state.....	26
5.2.3 Calculating the function $Q_i = f(\Delta p_i, R_i)$	27
5.2.4 Calculation $\frac{E}{V_i}$ from $Q_i = f(\Delta p_i, R_i)$	28
5.2.5 Estimating $\frac{E}{V_i R_i}$ with a least squares estimate.....	29
5.2.6 The effect of model and measurement errors	30
5.2.8 Conclusion.....	31
5.3 FRICTION.....	31
5.3.1 Calculation of friction	31
5.3.2 The Stribeck curve	33
5.3.3 Conclusion.....	33
5.4 IDENTIFICATION OF LOAD DYNAMICS.....	33
5.4.1 Frequency Response Function.....	33
5.4.2 Load characteristic.....	34
5.4.3 Conclusion.....	34
CHAPTER 6 CONCLUSIONS AND RECOMMENDATIONS	35

6.1 MEASUREMENTS.....	35
6.2 IDENTIFICATION.....	35
6.3 VALIDATION.....	36
BIBLIOGRAPHY	37
APPENDIX A THEORY OF THE MODEL.....	38
APPENDIX A.1 EFFECTIVE BULK MODULUS	38
APPENDIX A.2 ADDED MASS	39
APPENDIX A.3 EQUIVALENT MASS.....	40
APPENDIX A.4 LOWEST NATURAL FREQUENCY	40
APPENDIX B STRAIN GAUGES	42
B.1 THEORY OF STRAIN GAUGES	42
B.2 SOURCES OF ERRORS.....	44
B.3 LEVEL OF BENDING MOMENTS IN THE PISTON ROD.....	45
<i>B.3.1 Bending in vertical plane</i>	<i>45</i>
<i>B.3.2 Bending moments in horizontal plane.....</i>	<i>50</i>
APPENDIX C: EXPERIMENTS WITH TEST RODS.....	53
C.1 PURPOSE OF THE TEST MEASUREMENTS	53
C.2 EXPERIMENTS	54
C.3 CONCLUSIONS	55
APPENDIX D MEASUREMENT EQUIPMENT	56
D.1 PRESSURE TRANSMITTERS	56
D.2 ACCELEROMETER	57
D.3 STRAIN GAUGES AND AMPLIFIER.....	57
<i>D.3.1 strain gauges.....</i>	<i>57</i>
<i>D.3.2 Strain gauge amplifier.....</i>	<i>58</i>
D.4 LASER VIBROMETER	58
D.5 SIGLAB.....	59
<i>D.5.1 specifications</i>	<i>59</i>
<i>D.5.2 Offset drift.....</i>	<i>59</i>
APPENDIX E TECHNICAL DRAWINGS.....	60

Nomenclature

A	area [m ²]
c	slope parameter for the friction curve [m/s]
d	arm of the cylinder force to the centre of rotation of the lock gate [m]
E	modulus of elasticity [N/m ²], bulk modulus [N/m ²]
F	force [N]
F_w	friction force [N]
F_{ext}	external force on the piston [N]
F_s	static friction force [N]
F_c	coulomb friction force [N]
f	frequency [1/s]
h	height of lock gate under water [m]
I	moment of inertia [kg·m ²]
I_a	added moment of inertia [kg·m ²]
k	strain gauge factor [-], spring constant [N/m]
L	length of lock gate [m]
M	moment [Nm]
M, m	mass [kg]
M_{eq}	equivalent mass [kg]
p	pressure [Pa]
\dot{p} , dp	time derivative of pressure [Pa/s]
Q	flow [m ³ /s]
R	resistance parameter [Pa·s/m ³], electrical resistance [Ω]
R, r	radius [m]
S	stroke [m]
T_m	kinetic energy of mass [J]
T_f	kinetic energy of fluid [J]
t	time [s]
\dot{V}	time derivative of a volume [m ³ /s]
V	volume [m ³], potential energy [J], Poisson's ratio [-]
V_0	output of voltage [V]
V_s	supply voltage [V]
v	velocity [m/s]
w	viscous friction parameter [Ns/m], distributed weight [kg/m]
x, \dot{x}, \ddot{x}	position [m], velocity [m/s], acceleration [m/s ²]
δ	slope parameter for the friction curve [s/m]
$\varepsilon, \varepsilon_b, \varepsilon_b, \varepsilon_\theta, \varepsilon_n$	strain [-], longitudinal, bending, thermal, normal
φ	angle [rad]
μ	friction coefficient [-]
ν	poissons ratio [-]
θ	phase shift [rad]
ρ	density [kg/m ³]
σ_n	normal stress [N/m ²]
ω	radial frequency [rad/s]

other subscribts

A,a	base side of the cylinder
B,b	annular side of the cylinder
Li	internal leakage
Le	external leakage
s	in the hydraulic system

Introduction

Rexroth Hydraudyne is an international company that designs and manufactures hydraulic cylinders, together with the hydraulic systems and the controllers to operate them. In these cylinders, the friction force can be a large part of the total force. Consequently, friction influences the dynamical behaviour of the system. One of the problems encountered in this field is stick-slip vibration. Stick-slip may be interpreted such that “stick” is due to the higher static friction between the sliding surfaces and “slip” is due to the lower kinetic friction during the slip itself. Above some critical velocity, these vibrations will not occur.

Within the project ‘Friction Induced Vibrations’ at Rexroth Hydraudyne, simulation models are developed and a test rig is designed and build to measure friction of seals and bearings strips. The aim is to predict possible occurrence of stick-slip vibrations. The critical velocity is here of special interest.

A most simple model is to model only the cylinder. Question is whether this is a too simple presentation of reality. Can the hydraulic system really be neglected or does it influence the dynamic behaviour of the cylinder? And if so, how should it be modelled? Furthermore, the driven system (a bridge, a lock-gate etc.) also has its own dynamical behaviour and natural frequencies, which influence the behaviour of the cylinder.

The objective of this internship was to validate the simulation model by way of measurements on a cylinder. Measurements for this purpose were done on the south lock in Schellingswoude. This lock is part of the ‘Oranjesluizen’ in the Noordzee kanaal between Amsterdam and the IJsselmeer. It was chosen because of its easy accessibility and operation.

Measurements of the pressure in different places in the system, the position, velocity and acceleration of the piston and the force in the rod were done. The aim was to identify the parameters of the simulation model from these measurements.

In this report, the model and measurements are described and the efforts to identify the parameters are discussed. Some effort is made to also include the experiences and problems encountered with the measurements. Most of this can be found in the appendices.

In chapter 1, a description of the system is given, the simulation model of the cylinder is presented and a model for the hydraulic system is deduced. Also, the driven system is discussed. Chapter 2 explains what measurements have to be done to identify the parameters and the dynamic behaviour. In chapter 3, the measurement set up, sensors and measurement series are described. Chapter 4 discusses the efforts to make the whole set of measurements ready for analysis. Discussed are, among other things, the determination of zero points and the conversion from voltage signal to the actual measurement values. Chapter 5 contains the analysis of the measurements and possible determination of the parameters. Discussed consecutively are the hydraulic system, the dynamic behaviour of the lock gate and the friction. The conclusions and recommendations are given in chapter 6.

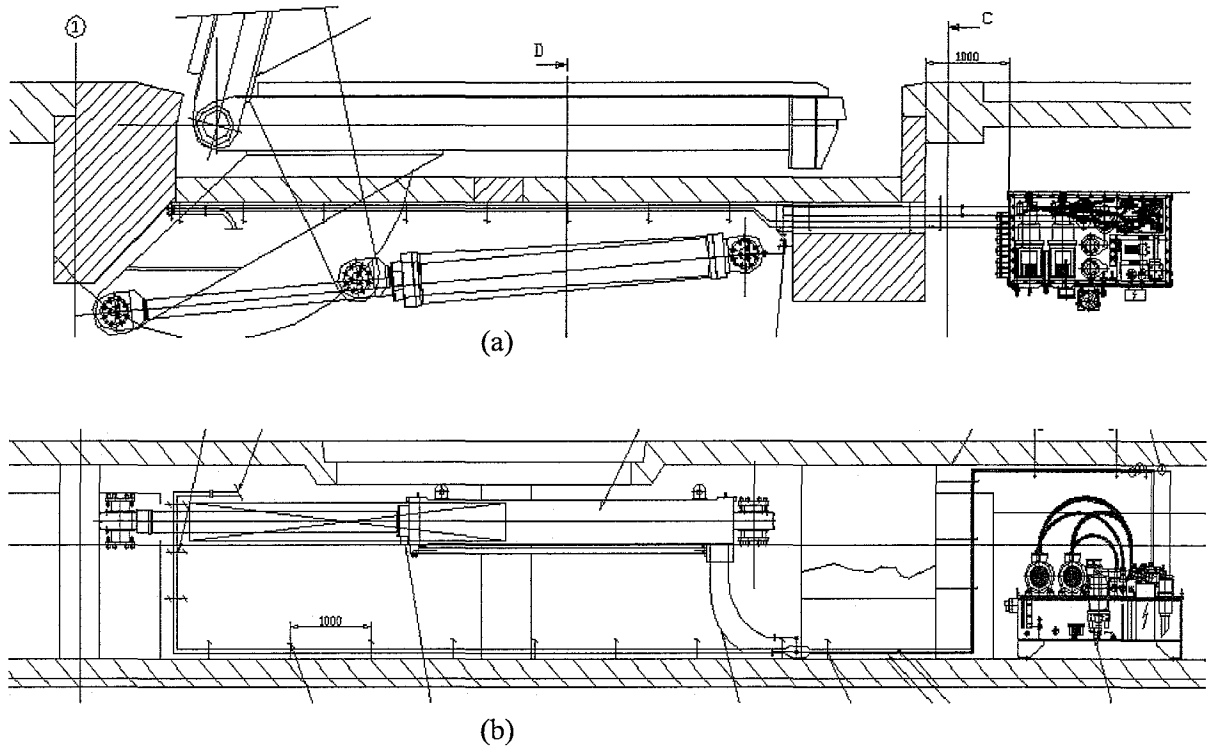


Figure 1.1 (a) Top view and (b) front view of the cylinder, lock gate and pump unit

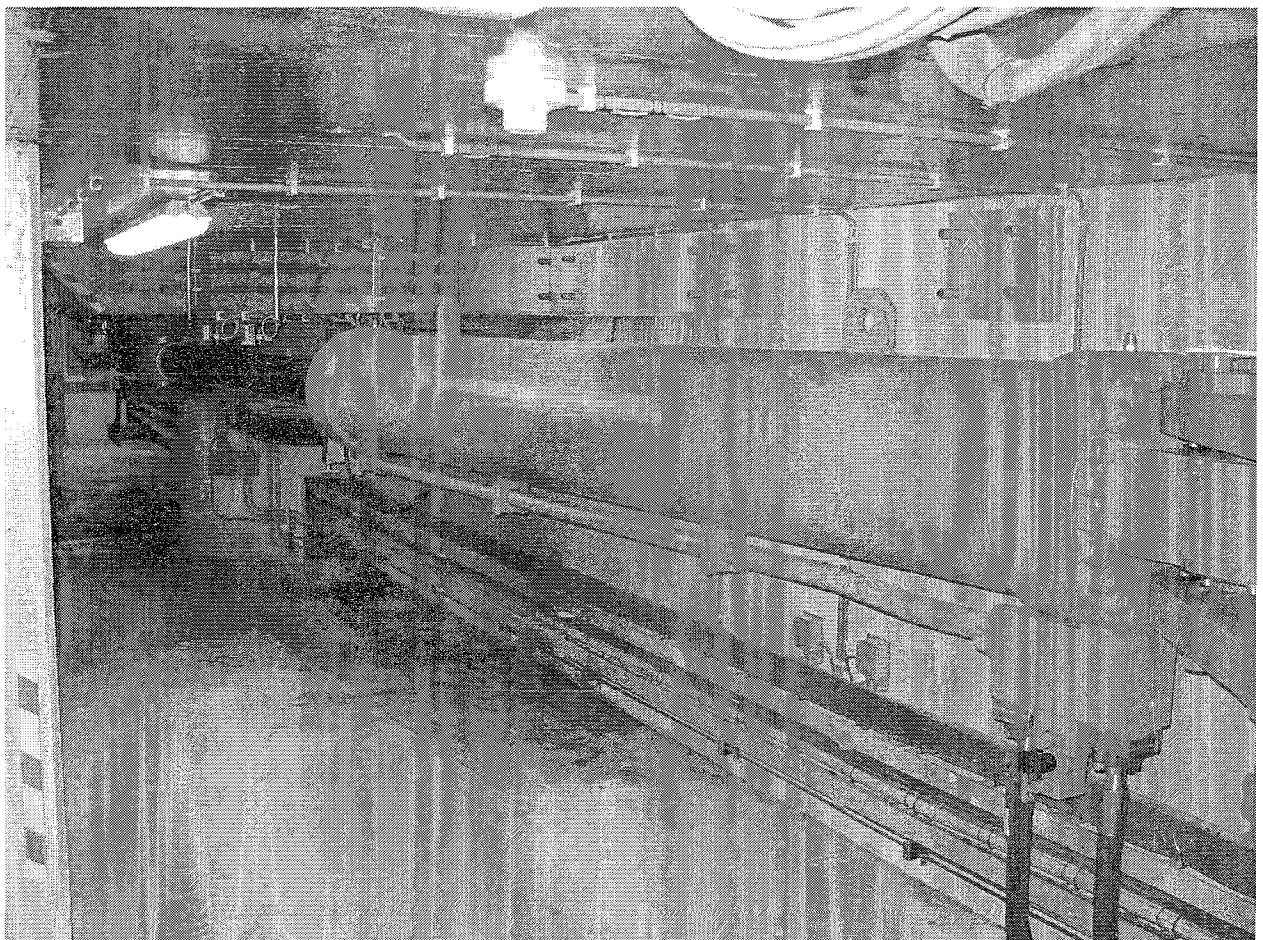


Figure 1.2 The cylinder

Chapter 1 Lock model

A model of the lock consists of a model of the cylinder, a model of the hydraulic system and a model of the driven system. The model of the cylinder does not depend on the application. It is enough to know whether it is a single or double acting cylinder. This model is the simulation model to be validated. The model of the hydraulic system does depend on the system in that is modelled, so the system will first be described, before the model of the hydraulic system is given. Since the driven system (lock gate) is often complicated to model, it is approached as a black box model. In paragraph 1.1 the system is described and in paragraph 1.2 the model of the cylinder, hydraulic system and the driven system are presented.

1.1 Description of the system

The system that is modelled is the low tide gate of the south lock of the 'Oranjesluizen' in Schellingwoude (Amsterdam). The 'Oranjesluizen' is a complex of locks between Amsterdam and the IJsselmeer. The lock gate on which the measurement where done is a spare gate, between the two gates which are normally used. During the measurements, the other lock gates were closed, so there is no current that influences the measurements.

One lock gate of the south lock is ca. 8 meter wide and ca. 7 meters high. It weighs 18 tons. A cylinder with an stroke of 3.2 m drives the door (see fig 1.1). The cylinder has a working stroke of 3.03 m and a diameter of the rod of 0.22 m. According to the instruction manual [Rex01], the normal load is 109 kN when opening the gate and 203 kN when closing the gate. The cylinder axis in normal use has a mean velocity of at least 23 mm/s and a maximum velocity of 100 mm/s. The cylinder is driven by a pump unit with two axial plunger pumps with variable delivery. The engine speed is 1000 rpm and the capacity at 1000 rpm is 70 l/m. The nominal engine power is 7.5 kW.

A SWKD card (sollwert karte digital) controls the slewing angle of the pumps. In normal operation the slewing angle of the pump follows the programmed velocity characteristic of the SWKD card. In emergency/maintenance operation, the slewing angle is controlled by a potentiometer in the control cabinet. In emergency/maintenance operation, the movement of the cylinder can be controlled from a control panel near the cylinder.

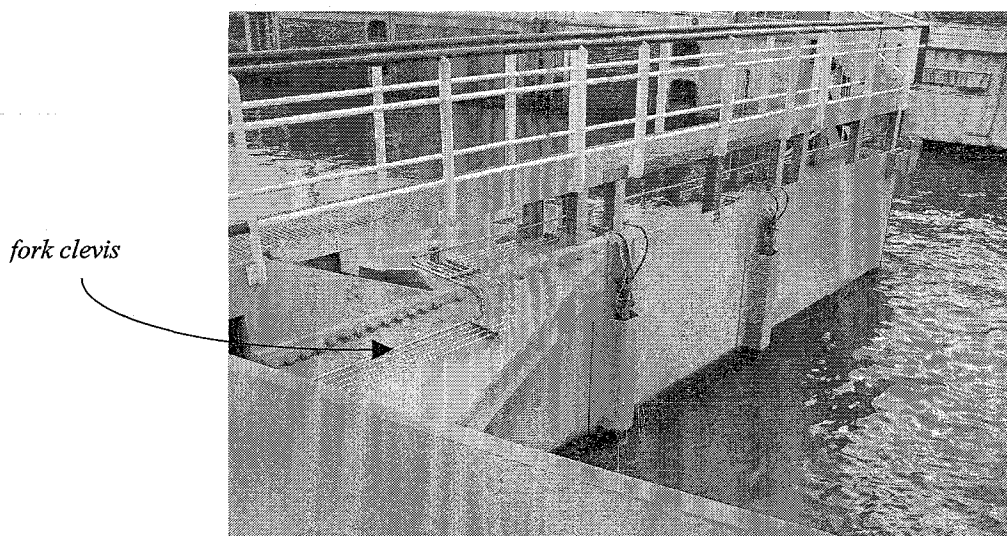


Figure 1.3 The lock gate

The cylinder is connected to the lock gate with a fork clevis (see fig 1.1 and 1.3). The hydraulic diagram of the system can be found in appendix [E]. When the lock gate is closing, the cylinder is moving inward. The flow of the bottom side flows to the tank. When the lock gate is opening, the cylinder is moving outward and the oil from the annular side flows to the bottom side: it is connected differentially. Figure (1.4) shows the main features for the two situations. The brake valves, in normal use, are completely open.

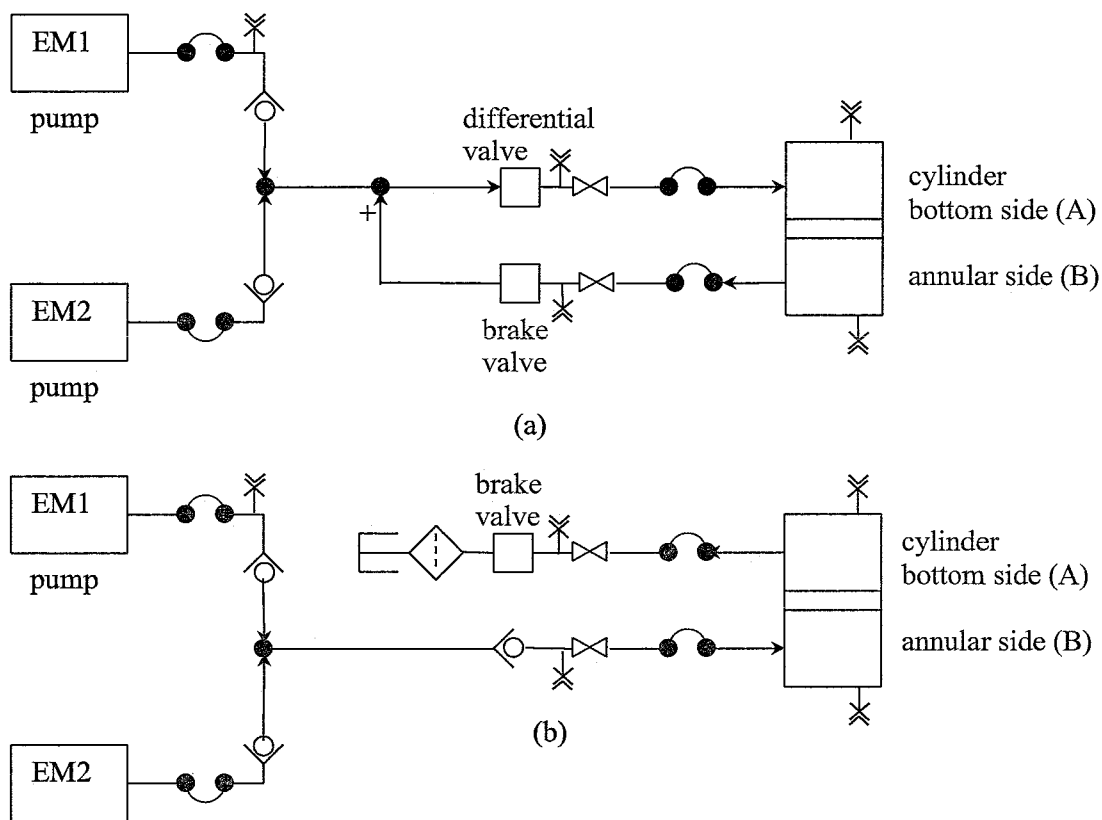


Figure 1.4: Impression of the hydraulic scheme. When the piston moves outward, (a) is the situation, when the piston moves inward (b) is the situation.





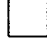

	flexible hose
	check valve
	minimess connection for pressure measurements
	manual valve
	cartridge valve
	filter

Table 1.1: Explanation of symbols used in Figure 1.4

1.2 Model of the lock

1.2.1 Model of the cylinder

The cylinder of the lock is a double acting cylinder. The model of the cylinder consists of the pressure dynamics and the equations of motion of the piston [Jel03]. The model described in this paragraph is the simulation model.

Pressure dynamics

From the equation of conservation of mass, the pressure dynamics of the cylinder can be modelled. Presuming a constant density and bulk modulus, the equation of conservation of mass yields

$$\sum Q_{in} - \sum Q_{out} = \dot{V} + \frac{V}{E} \dot{p} \quad (1.1)$$

where V is the volume of the fluid, Q is the volume flow, p is the pressure and E is the effective bulk modulus (app [A.1]).

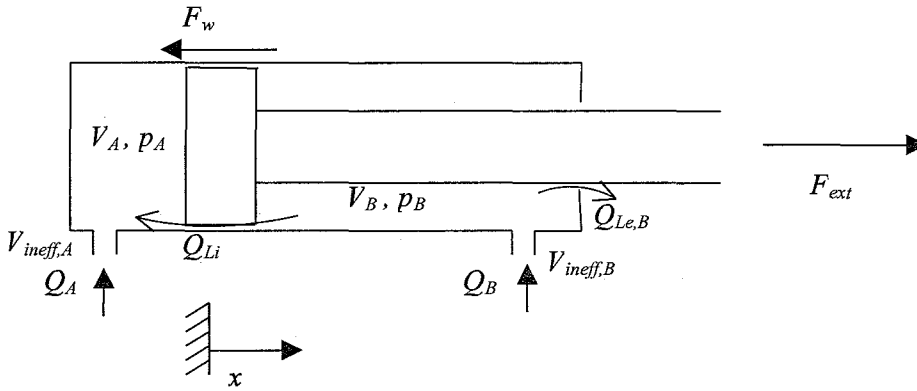


Figure 1.5 Double acting cylinder

From equation (1.1) and figure (1.) yields the pressure dynamics of the cylinder.

$$\dot{p}_A = \frac{E}{V_A(x) + V_{ineff,A}} (Q_A - \dot{x} \cdot A_A + Q_{Li}) \quad (1.2)$$

$$\dot{p}_B = \frac{E}{V_B(x) + V_{ineff,B}} (Q_B + \dot{x} \cdot A_B - Q_{Li} - Q_{Le,B}) \quad (1.3)$$

Here, V_A is the effective volume of bottom chamber (the volume required to fill the chamber), V_B is the effective volume of the annular chamber, V_{ineff} is the ineffective volume on side A or B (pipelines, buffer volumes etc.) and A_A and A_B respectively the bottom and annular area.

When the internal and external leakage are neglected, the pressure equations come to

$$\dot{p}_A = \frac{E}{V_A(x) + V_{ineff,A}} (Q_A - \dot{x} \cdot A_A) \quad (1.4)$$

$$\dot{p}_B = \frac{E}{V_B(x) + V_{ineff,B}} (Q_B + \dot{x} \cdot A_B). \quad (1.5)$$

Equation of motion of the piston

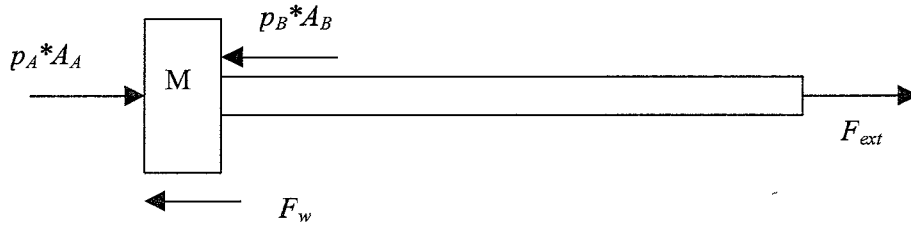


Figure 1.6 Forces on the piston

Figure (1.6) shows all the forces that act on the piston. The equation of motion of the piston now becomes

$$M \cdot \ddot{x} = p_A \cdot A_A - p_B \cdot A_B - F_w + F_{ext} \quad (1.6)$$

Mass

The mass M in the equation of motion is the total mass of the moving parts. It consists of the mass of the piston and the mass of the fluid on side A and B.

Friction

One of the main non-linearities in the cylinder model, is the non-linear friction. A practical way to model friction is by way of the Stribeck curve (fig (1.7)). This curve can be approximated with a mathematical equation. In the model used for simulating stick-slip vibrations, equation (1.7) was chosen. Another way to represent the Stribeck curve is equation (1.8).

$$F_w = \left(\frac{F_s - F_c}{1 + \delta \cdot |\dot{x}|} + F_c \right) \cdot \text{sgn}(\dot{x}) + w \cdot \dot{x} \quad (1.7)$$

$$F_w = \left[(F_s - F_c) \exp\left(-\frac{|\dot{x}|}{c}\right) + F_c \right] \text{sgn}(\dot{x}) + w \cdot \dot{x} \quad (1.8)$$

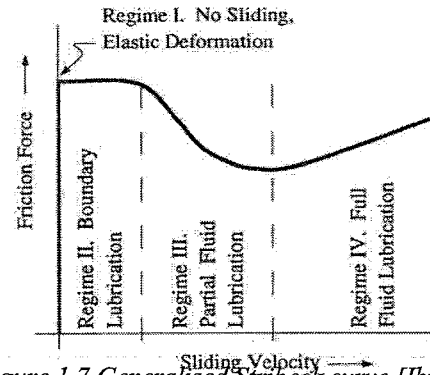


Figure 1.7 Generalised Stribeck curve [Ibr92]

In these equations, F_s denotes the static friction force, F_c the kinetic friction force, w is the viscous friction parameter and δ and c are slope parameters. The main difference between these methods is the way the slope for low velocities is modelled. In these model representations, possible asymmetry between the friction forces and temperature dependence are not taken into account. This can give a significant difference in the friction parameters.

1.2.2 Model of the hydraulic system

When only the cylinder is modelled, the flow would be considered constant and proportional with the slewing angle of the pumps. When the dynamics of the hydraulic system are much faster than the dynamics of the cylinder, this is allowable. If the dynamics of the hydraulic system and cylinder have a time constant of the same order of magnitude, the dynamics of the hydraulic system will have to be taken into account.

Simple lumped volumes model

To determine the time constant of the hydraulic system, it is modelled as a series of volumes and resistance's. These resistance's can be linear or quadratic with the flow. The linear model describes pipelines and the quadratic model describes throttles. Both are present in the hydraulic system, so the

expected model is a combination of these two. The inertia of the oil is neglected here. Experiments will show whether this is an allowable neglectance.

From figure (1.4) the block scheme of the hydraulic system can be constructed. The equations for the volumes are deducted from equation (1.1). Since the volumes in the hydraulic system are constant, equation (1.1) can be rewritten to

$$\dot{p} = \frac{E}{V} (Q_{in} - Q_{out}) \quad (1.7)$$

A linear relationship between the pressure loss and the flow gives equation (2.2) and a quadratic relationship gives equation (1.8).

$$Q = \frac{\Delta p}{R} \quad (1.8)$$

$$Q = \frac{\sqrt{\Delta p}}{R} \quad (1.9)$$

In figure 1.9 and 1.10, the block schemes and equations of the models for the inward and outward movement are presented.

Shortcomings

The model of the hydraulic system presented above is a very simple representation of reality. In reality inertia effects can be present over the pipelines. A lumped parameter model is assumed instead of continuous distributed parameters. Also, the scheme in figure (1.4) is a short representation of the hydraulic scheme (appendix [E]).

1.2.3 Model of the driven system

The driven system, the lock gate, will be approached as a black box. From the measurements of the force in the rod and the movement of the piston, a response of the force on the measured movement will be searched for. The aim is to find a representation that can be build in into the simulation model.

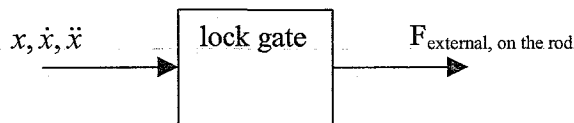
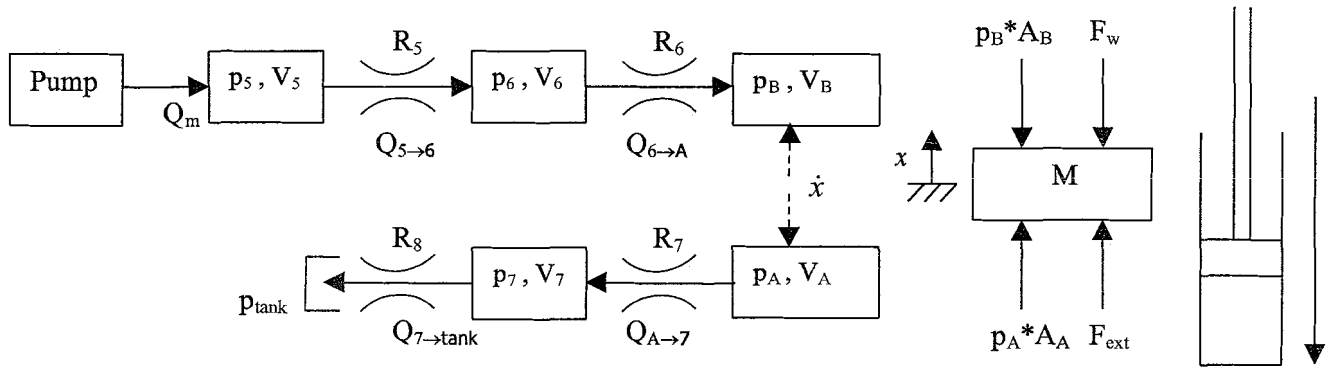


Figure 1.8 Black box modelling of the lock gate.

Figure 1.9 Model for inward moment of the cylinder, closing the lock gate.



With:

$$\dot{p} = \frac{E}{V} (Q_{in} - Q_{out})$$

linear resistance:

$$Q_{5 \rightarrow 6} = \frac{p_5 - p_6}{R}$$

quadratic resistance

$$Q_{5 \rightarrow 6} = \frac{\sqrt{p_5 - p_6}}{R}$$

$Q_{5 \rightarrow 6}$ is the flow from Volume 5 to Volume 6. The flow from V_6 to V_5 is $Q_{6 \rightarrow 5} = -Q_{5 \rightarrow 6}$

$$\dot{p}_5 = \frac{E}{V_5} (Q_m - Q_{5 \rightarrow 6})$$

$$M \cdot \ddot{y} = p_A \cdot A_A - p_B \cdot A_B - F_w + F_{ext}$$

$$\dot{p}_6 = \frac{E}{V_6} (Q_{5 \rightarrow 6} - Q_{6 \rightarrow B})$$

$$F_w = \left(\frac{F_s - F_d}{1 + \delta \cdot |\dot{y}|} + F_d \right) \cdot \text{sign}(\dot{y}) + w \cdot \dot{y}$$

$$\dot{p}_B = \frac{E}{V_B} (Q_{6 \rightarrow B} - \dot{y} \cdot A_B)$$

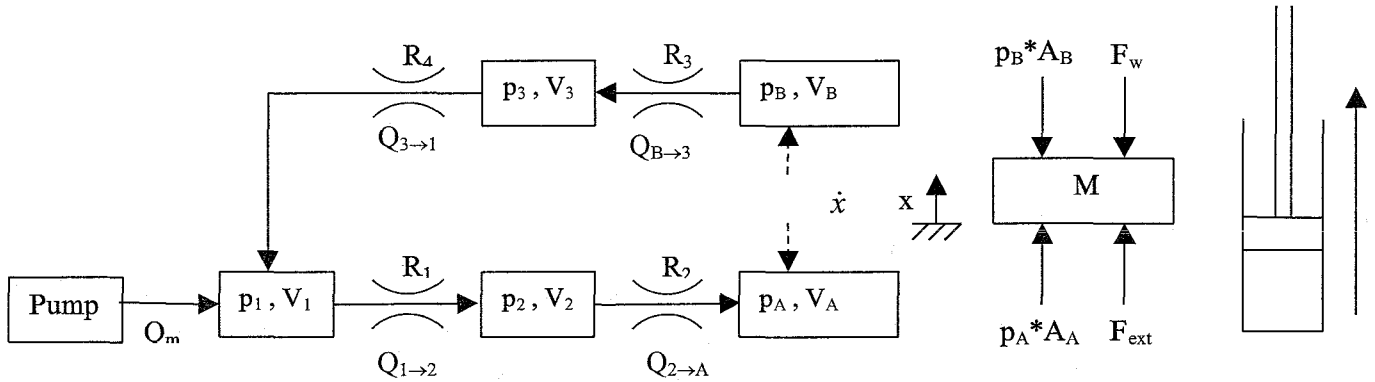
$$F_{ext} = f(y, \dot{y}, \ddot{y})$$

$$\dot{p}_A = \frac{E}{V_A} (\dot{y} \cdot A_A - Q_{A \rightarrow 7})$$

In Simulink model, $Q_A = Q_{7 \rightarrow A}$

$$\dot{p}_7 = \frac{E}{V_7} (Q_{A \rightarrow 7} - Q_{7 \rightarrow t})$$

Figure 1.10 Model for outward moment of the cylinder, opening the lock gate.



With

$$\dot{p} = \frac{E}{V} (Q_{in} - Q_{out})$$

linear resistance:

$$Q_{1 \to 2} = \frac{p_1 - p_2}{R}$$

quadratic resistance:

$$Q_{1 \to 2} = \frac{\sqrt{p_1 - p_2}}{R}$$

$Q_{1 \to 2}$ is the flow from Volume 1 to Volume 2. The flow from V_2 to V_1 is $Q_{2 \to 1} = -Q_{1 \to 2}$

$$\dot{p}_1 = \frac{E}{V_1} (Q_m + Q_{3 \to 1} - Q_{1 \to 2})$$

$$M \cdot \ddot{y} = p_A \cdot A_A - p_B \cdot A_B - F_w + F_{ext}$$

$$\dot{p}_2 = \frac{E}{V_2} (Q_{1 \to 2} - Q_{2 \to 3})$$

$$F_w = \left(\frac{F_s - F_d}{1 + \delta \cdot |\dot{y}|} + F_d \right) \cdot \text{sign}(\dot{y}) + w \cdot \dot{y}$$

$$\dot{p}_A = \frac{E}{V_A} (Q_{2 \to 3} - \dot{y} \cdot A_A)$$

$$F_{ext} = f(y, \dot{y}, \ddot{y})$$

$$\dot{p}_B = \frac{E}{V_B} (\dot{y} \cdot A_B - Q_{B \to 3})$$

In the Simulink model, $Q_B = Q_{3 \to B}$

$$\dot{p}_3 = \frac{E}{V_3} (Q_{B \to 3} - Q_{3 \to 1})$$

Chapter 2 Measurement setup for identification of the parameters

With the models from chapter 1, a measurement setup can be designed for identification of the parameters.

Identification of friction

The friction force itself is not measurable, but all the other variables from the equation of motion (eq (1.6)) can be measured and the bottom area (A_A) and the annular area (A_B) are known. The equation of motion can be rewritten to

$$F_w = p_A \cdot A_A - p_B \cdot A_B + F_{ext} - M \cdot \ddot{x} \quad (2.1)$$

The friction calculated from equation 2.1 is the friction in the cylinder. The variables to be measured are the pressure on the bottom and annular side, the acceleration of the piston and the force in the rod. The measurements of the pressures can be done with simple pressure transducers. Connections for these transducers are present on the cylinder. The acceleration can be measured with an accelerometer and the force in the rod can be measured with strain gauges. Care has to be taken to measure only the axial force and acceleration.

Identification of E , V_i and R_i

When the pressure variations are damped out and the pressure is constant, the flow is constant over the hydraulic system and the resistance's can be determined, since

$$\dot{p}_i = \frac{E}{V_i} (Q_{in,i} - Q_{out,i}) \quad (2.2)$$

and

$$Q_i = f(\Delta p_i, R_i)$$

When these resistance's are known, the quotients $\frac{E}{V_i}$ can be determined from the calculated flow and the time derivative of the pressure. For this process, the pressures in the system and the velocity of the piston have to be measured.

Identification of the black box model of the lock gate

Identification of the dynamic behaviour of the lock gate is not simple. The behaviour is expected to be non-linear and dependent on position and velocity of the piston because the resistance of water is not linear with the velocity and depends on the position of the lock gate with respect to the wall. A simple dynamic transfer between the movement and the force in the rod will therefore not be sufficient or perhaps not even possible, when the non-linear behaviour is too dominant. Another way to represent the reaction of F_{ext} on the movement of the cylinder is by way of characteristic curves. For instance, a plot of F_{ext} against the velocity for different positions can give much information about the dependence of F_{ext} on the velocity and position.

Chapter 3 Measurements on the lock

The purpose of the measurements was to determine the parameters in the model and the dynamic behaviour of the lock gate. To achieve this, the following measurements were done.

- The pressure on the bottom side of the cylinder (p_A),
- the pressure on the annular side of the cylinder (p_B),
- the pressure on three places in the hydraulic system,
 - close after the pump (p_P),
 - just before the oil leaves the hydraulic power pack into the pipes connected to bottom and on annular side (p_{As} and p_{Bs}),
- the displacement of the piston (x),
- the velocity of the piston (\dot{x}),
- the acceleration of the piston (\ddot{x}),
- the force in the rod (F_{ext}).

Measurements were done at different positions and velocities to capture position and velocity-dependant behaviour. Next to these signals, the control signal of the pump was measured. This signal controls the slewing angle of the pump and therefore it is a set point for the velocity of the piston.

In the following paragraphs will be described how these measurements were done. In paragraph 3.1 the measurement equipment and the placement of the sensors is described and in paragraph 3.2 the data acquisition and chosen settings are discussed. In paragraph 3.3 the measurement series are presented.

3.1 Measurement equipment and placement

In this paragraph a short description of the measurement equipment and settings is given. Specification and information about calibration can be found in appendix [D].

Pressure transducers

The pressure transducers used for the measurements are 400 bar pressure transducers with a 4-20 mA output. Minimes connections for pressure measurements were used in the hydraulic system.

Accelerometer

An accelerometer that measures acceleration ($\pm 5g$) in one direction was used for the measurement of the acceleration of the piston. It gives an output of 4-20 mA. It was glued horizontally on the clevis (fig 3.1).

Strain gauges

The force in the rod was measured with strain gauges. A full Wheatstone bridge with 4 active strain gauges was built in a way to compensate for bending moments and thermal strain (see appendix [B]). The strain gauges were glued on the sides of the piston at circa 60 cm from the clevis to avoid measuring at a stress concentration of the thread in the clevis. A strain gauge amplifier was used to exit the bridge and convert the mV output of the bridge to a larger voltage. It was set to a sensitivity of 0.23 mV/V and calibrated with a 5 M Ω shunt resistance. The low pass filter in the amplifier was set at 10 Hz.

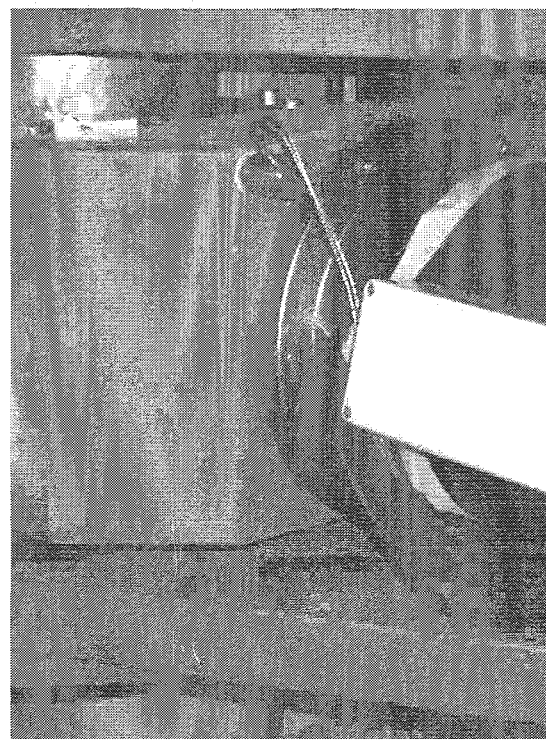


Figure 3.1 Mounting of the accelerometer on the clevis

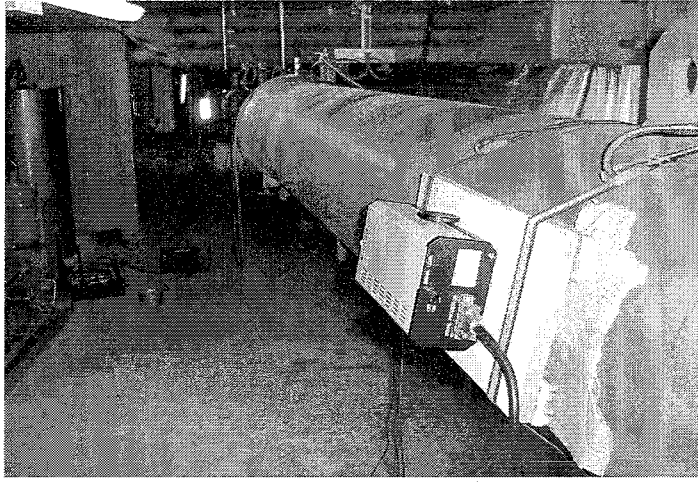


Figure 3.2 Mounting of the laser head on the shell

Laser vibrometer

A laser vibrometer measured the axial velocity and displacement of the clevis. The laser head was mounted on the shell and a block with reflecting tape was mounted on the clevis. The measurement range used for the displacement was 1.3 mm (the largest available). The range was increased with an automatic reset signal. The measurement sensitivity used for the velocity was 125 mm/s/V. This was the only range that could measure DC [appendix D]. The filters of the vibrometer were set on off.

CIMS

CIMS (Ceramax Integrated Measuring System) is a position-measuring device on the cylinder. The cylinder has, under the CERAMAX layer on the piston, a groove pattern with 1 cm wide grooves, which approximate a cosine. Magneto resistive elements on 2 locations, shifted 90° (0.25 cm) generate a quasi sine and cosine signal. These signals can be transformed into quadrature pulses. In the CIMS measuring system, 1024 pulses are generated every cm. The linearity is limited to ± 1 mm, due to the deviation of the signals with respect to exact sine and cosine signals. The pulses are converted to a 4-20 mA signal with a converter (module for CIMS Mk II). The DA converter bits limit the accuracy to 0.03% of full stroke.

3.2 Data acquisition

The system used for data-acquisition is SigLab. SigLab is a data acquisition and analyser system that allows data acquisition on 16 channels with simultaneous sampling. An anti-aliasing filter is built-in and each channel has a 16 bit AD-converter. It measures voltage signals and the range can be chosen between ± 20 mV and ± 10 V and. SigLab can be operated directly under MATLAB.

Since SigLab measures only voltage signals and most sensors produce a 4-20 mA signal, these signals were converted a 2-10 V signal with a shunt resistance of 500 Ohm $\pm 0.05\%$. The measurement voltage range for each channel was set as tight as possible to make the best use of the 16 bit AD-converter. Most signals have a dc offset. This offset is caused by the conversion from current to voltage signal and by an offset in the sensor output. It limits the resolution. For instance, since the accelerometer signal has an dc offset of 6 V, the ± 10 V range had to be used. This limits the resolution to 0.3 mV.

In [Jel03] a sampling interval of $1/6 - 1/10$ of the time constant of the system is suggested. Since τ_{63} from most measurements is around 1 second, this would mean a desired bandwidth of ca. 10 Hz. The sampling frequency has to be ca 2.5 times the desired bandwidth of the measurements, because the anti-aliasing filter in SigLab is a low pass filter with a cut off frequency of ca 0.5 x the sampling frequency. Since a frequency of ca 17 Hz was present in some of the measurements, a sampling frequency of 51.2 Hz was chosen. Signals up to ca 25 Hz can be measured now. This also gives the advantage that distortions of 50 Hz are repressed. Distortions of 50 Hz are often present in measurement signal, because electro magnetic fields from power cables and systems can disturb the measurement signals.

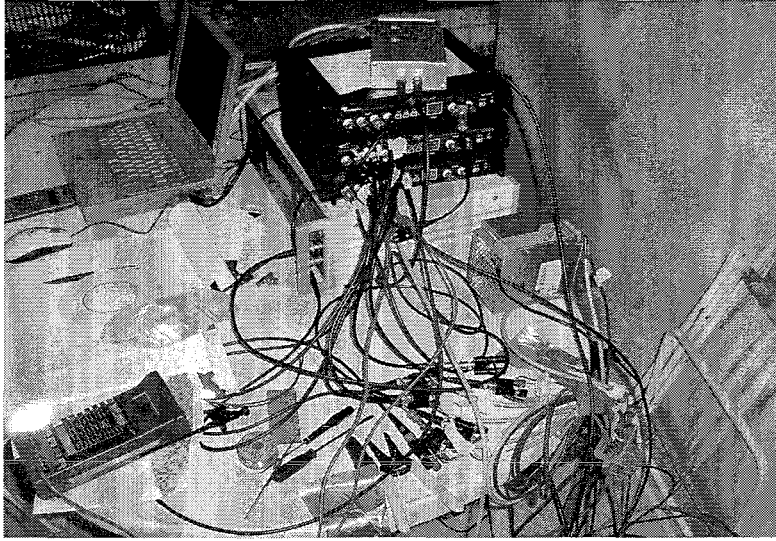


Figure 3.3 Data acquisition

3.3 Measurements

Before the measurement series were started, a measurement was done of the zero point of SigLab and the zero point of the pressure transducers.

The measurements on the lock were done with 4 different control signals: 1, 3, 5, and 7 Volt. 0 Volt is a slewing angle of 0 degrees, 10 V is a maximum slewing angle. The slewing angle of the pump controls the input flow of the system and thus the velocity of the piston. With the same control signal, the outward velocity is larger than the inward velocity, because with an outward movement the system is connected differentially and the oil from the annular side flows to the bottom side, and not to the tank.

For each control signal, start and stop responses were measured on different positions. The CIMS signal was used to determine the positions. Since the strain gauges were glued on the rod at ca 60 cm from the clevis, it was not possible to use the entire stroke of the cylinder. The remaining stroke was divided in 5 parts. This gave 5 start/stop responses in each direction. Each measurement was done 4 or 5 times. Also measurements of complete runs were made.

Between the stop and starts, a waiting period of ca 20 seconds was used. A time of ca 10-20 seconds is necessary to make a good estimation of the low frequencies of the signal. Since the running time between two positions with a control signal of 7 V was too short, start and stop responses with this control signal were measured on only 3 positions.

Summarized:

Start and stop responses were measured on:

Control signal [V]	position [m] from clevis
1	0.8, 1.2, 1.6, 2.0, 2.4, 2.8
3	0.8, 1.2, 1.6, 2.0, 2.4, 2.8
5	0.8, 1.2, 1.6, 2.0, 2.4, 2.8
7	0.8, 1.8, 2.8

Table 3.1 Measurement series

In the following chapters, sometimes is spoken about “experiments”. With experiments series of start and stop responses are meant. They are chronological in time. In total, 23 experiments were done that incorporated ca. 350 step responses.

Chapter 4 Pre-processing the data

In paragraph 4.1, some tools for processing and analysis of the data are presented. In paragraph 4.2 the pre-processing of the data is described. More information can be found in [Den98].

4.1 Tools for signal analysis

Frequency domain representation

It is often convenient to characterise signals in the frequency domain instead of the time domain. This means that the signal is written in terms of the frequencies that it contains. For representing the signal in a plot, the x-axis will then be a frequency axis, instead of a time axis. For instance, the signal

$$S(t) = A \cdot \cos(\omega t + \theta) \quad (41)$$

can be represented by the a frequency ω in rad/s with amplitude A and phase θ . In a plot this looks like figure (41). This is called an amplitude and a phase spectrum. The conversion from time domain to frequency domain is called a Fourier Transform. All signals can be represented as a combination of different sines and cosines. Instead of an amplitude spectrum, often a power spectral density (PSD) spectrum is used. In this spectrum not amplitude A , but A^2 is used.

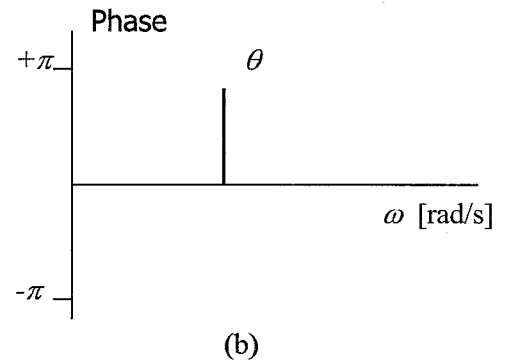
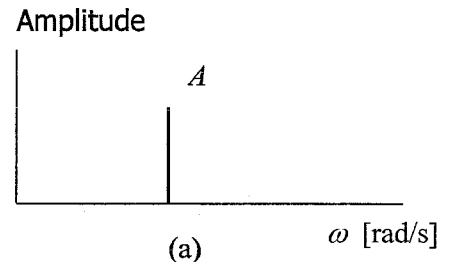


Figure 4.1 (a) amplitude and (b) phase spectrum of $A \cdot \cos(\omega t + \theta)$

Frequency Response Function (FRF)

A characteristic of a linear system is that the output signal is a linear combination of the frequencies of the input signal.

This means that if the amplitude of a frequency in the input signal is doubled, the amplitude of that frequency in the output signal is also doubled. Because of this characteristic, a transfer function can be determined. A transfer function represents the relation between 2 signals. In the frequency domain, equation 42 holds. Here, with the capitals, the Fourier Transform of the signals x and y are meant. $H(f)$ is the transfer function. Conveniently, in the frequency domain the input signal x can be multiplied by the transfer function to obtain the output signal y .

$$Y(f) = H(f) * X(f) \quad (42)$$

This transfer function is usually plotted in the frequency domain in a Bode diagram (fig 4.2). A Bode diagram contains an amplitude plot and a phase plot that represent the complex transfer function $H(f)$. The Frequency Response Function (FRF) is the transfer function evaluated over the imaginary axis. It assumes that it is build from sines with constant amplitude (no damping).

Coherence

A FRF only has meaning if the two signals are linearly related to each other. The coherence is a measure for the correlation between two signals. A coherence of 1 means a large correlation, a coherence of 0 means no correlation. This coherence is determined for all frequencies.

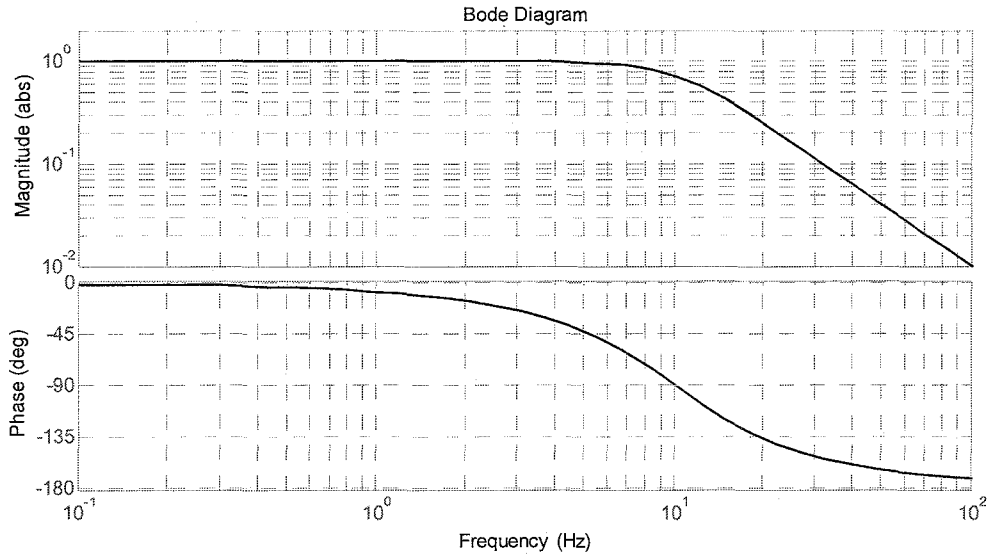


Figure 4.2 Example of a low pass filter in a Bode diagram. This is a continuous second order filter with a cut off frequency of 10 Hz.

Filtering

Filtering can be done before or after sampling. Before sampling, the data is filtered analog, using analog electronics. After sampling, the measurements can be filtered digitally, by computer. The reason is often to remove noise from the data. Normally, this is done with a low pass filter, a filter that lets only low frequencies through. High frequencies are repressed. MATLAB contains a lot of routines that design low pass filters. Two important choices for a low pass filter are the cut off frequency and the order of the filter.

The cut off frequency determines from what frequency the frequencies are repressed and the order determines how much they are suppressed. A filter can be characterised in a bode plot (fig 4.2).

Further subjects

Two other subjects in signal analysis are windowing and anti-aliasing. It is beyond the scope of this report to explain these subjects in detail. These subjects are discussed in [Den98].

4.2 Pre-processing the data

To make the data more manageable, the data has been put into a data structure in MATLAB. With help of the measured control signal, the data was cut into ca 350 stop and start responses. The DC-offsets were removed and the voltage signals were converted into the actual measurement values. In the following paragraphs this process is described for each signal and some remarks are made about the error in the measurements. Figure 4.9 gives an example of the measurements.

4.2.1 The velocity measurements

DC offset

The vibrometer signal showed a nonconstant DC offset of ca. 0.15 V. If for each experiment separately a DC offset was determined, figure (4.3) was obtained. It is known that certain measurement

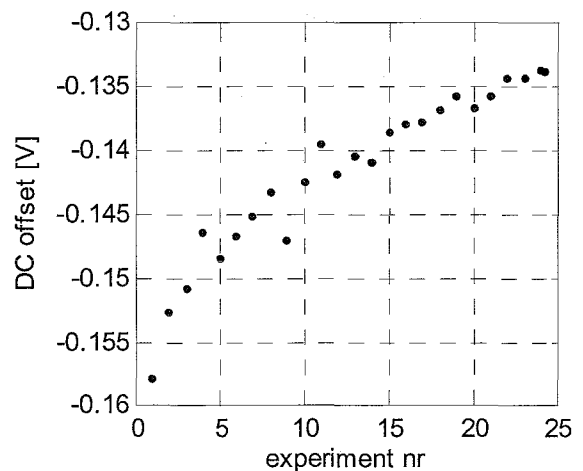


Figure 4.3 DC offset in the vibrometer's velocity signal

devices drift with temperature. The measured drift cannot be explained by the warming up of the laser head, because after 5 hours, it is still changing.

The measurements were corrected for the DC offset determined for each experiment.

Sensitivity

The sensitivity of the vibrometer was set to 125 mm/s/V. This is the least sensitive setting of three settings. Ideally, the most sensitive one should have been used. However, not all sensitivities could measure a constant velocity (they were AC coupled). Only the least sensitive state was able to measure constant velocities. This meant less resolution in the measurements.

Filtering

In the measurement of the velocity, often spikes were present. At these points the laser lost signal for a short while and registers a spike in the velocity. The spikes were numerically cut out and a low pass filter was used to smoothen the results.

A typical measured velocity is ca 15 mm/s with overshoot to 20 mm/s.

4.2.2 The displacement measurement with the laser vibrometer

Originally, a laser vibrometer with a displacement range of 8.2 cm would have been used, but due to circumstances, a laser vibrometer with a displacement range of 13 mm was used. The displacement range can be reset, so a larger displacement can be measured. However, this gives distortions in the reconstructed signal. Since this distortion was present every 13 mm, it was not possible to reconstruct a usable signal and the displacement signal of the laser vibrometer is not used.

4.2.3 Displacement measurement with the CIMS

In paragraph 3.1 it was explained that the CIMS signal is not an accurate measurement (see paragraph 3.1). However, it can be used to determine the position of the piston for determining position dependencies. The CIMS signal gives a 4 to 20 mA signal over the entire stroke.

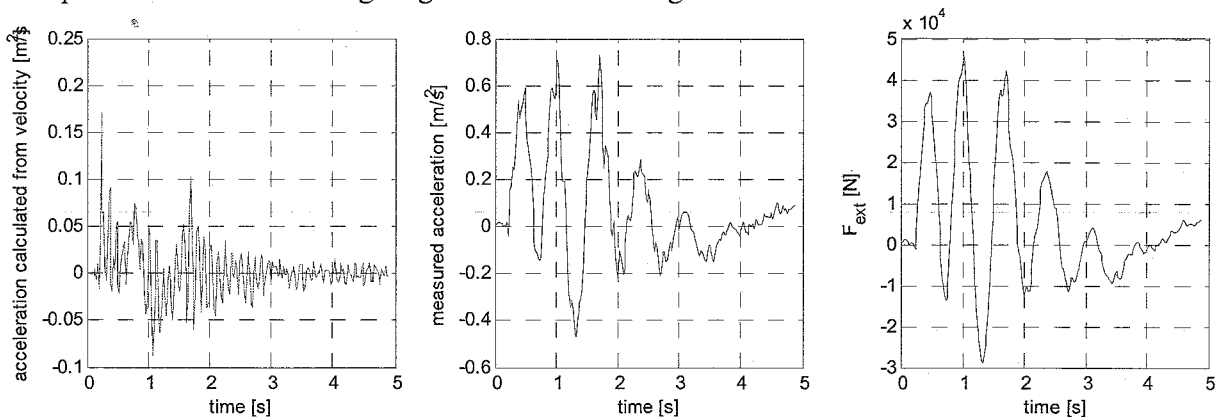


Figure 4.3: (a) time derivative of the velocity [m/s^2] (b) acceleration from accelerometer [m/s^2] (c) Force in the rod [N]

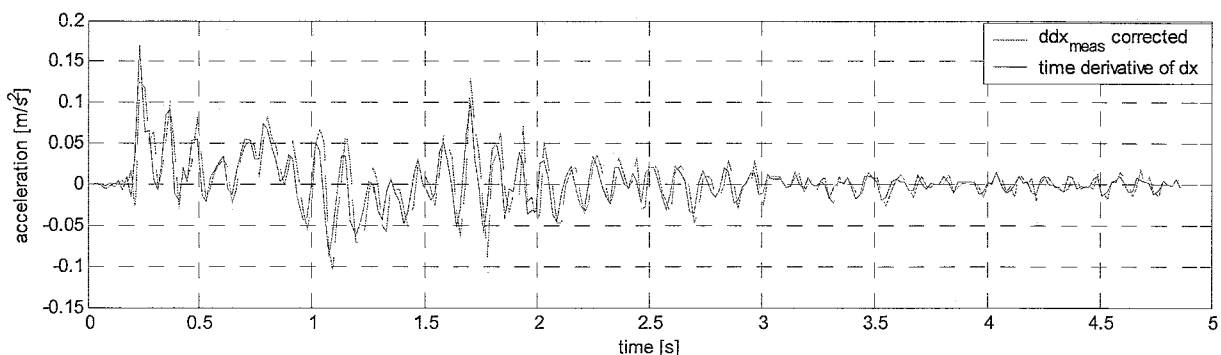


Figure 4.4 Comparison of the time derivative of the velocity and the corrected acceleration from the accelerometer [m/s^2].

4.2.4 The acceleration measurements

DC offset

The DC offset on the acceleration signal was determined from the acceleration signal when the cylinder was not moving. The DC offset after conversion to Volts, was 6.15 V. Since 5.95 V is 0 g ($g = 9.81 \text{ m/s}^2$), the DC offset was 0.25 g. This means the accelerometer was not aligned horizontally. It was ca 14° out of alignment. If this was a constant offset, it would not be a problem.

Sensitivity

The sensitivity of the accelerometer is 0.8 V/g, which is $0.0815 \text{ V}/(\text{m/s}^2)$.

Distortions of the signal

When the velocity signal is differentiated, it is not consonant with the acceleration. Both the shape and the amplitude do not coincide (see fig 4.4 (a) and (b)). This means that not the axial acceleration is measured. Since the shape of the acceleration signal is almost the same as the external force signal, it can be expected that the source of the distortion of the acceleration signal is proportional with the external force.

Figure 4.6 shows the FRF of F_{ext} over \ddot{x} . It is constant at $8 \cdot 10^4$ over all frequencies up to ca 6 Hz. The coherence is also good up to 6 Hz. This could falsely be interpreted as a stiff coupled mass of 80 tons. Since it was shown above that the acceleration signal was not the axial acceleration, this would be a wrong conclusion. However, the result can be used to correct the acceleration measurement. If the external force divided by the transfer factor mentioned above is subtracted from the measured acceleration signal (eq 4.1), the real acceleration remains. It coincides almost exactly with the differentiated velocity (fig 4.5).

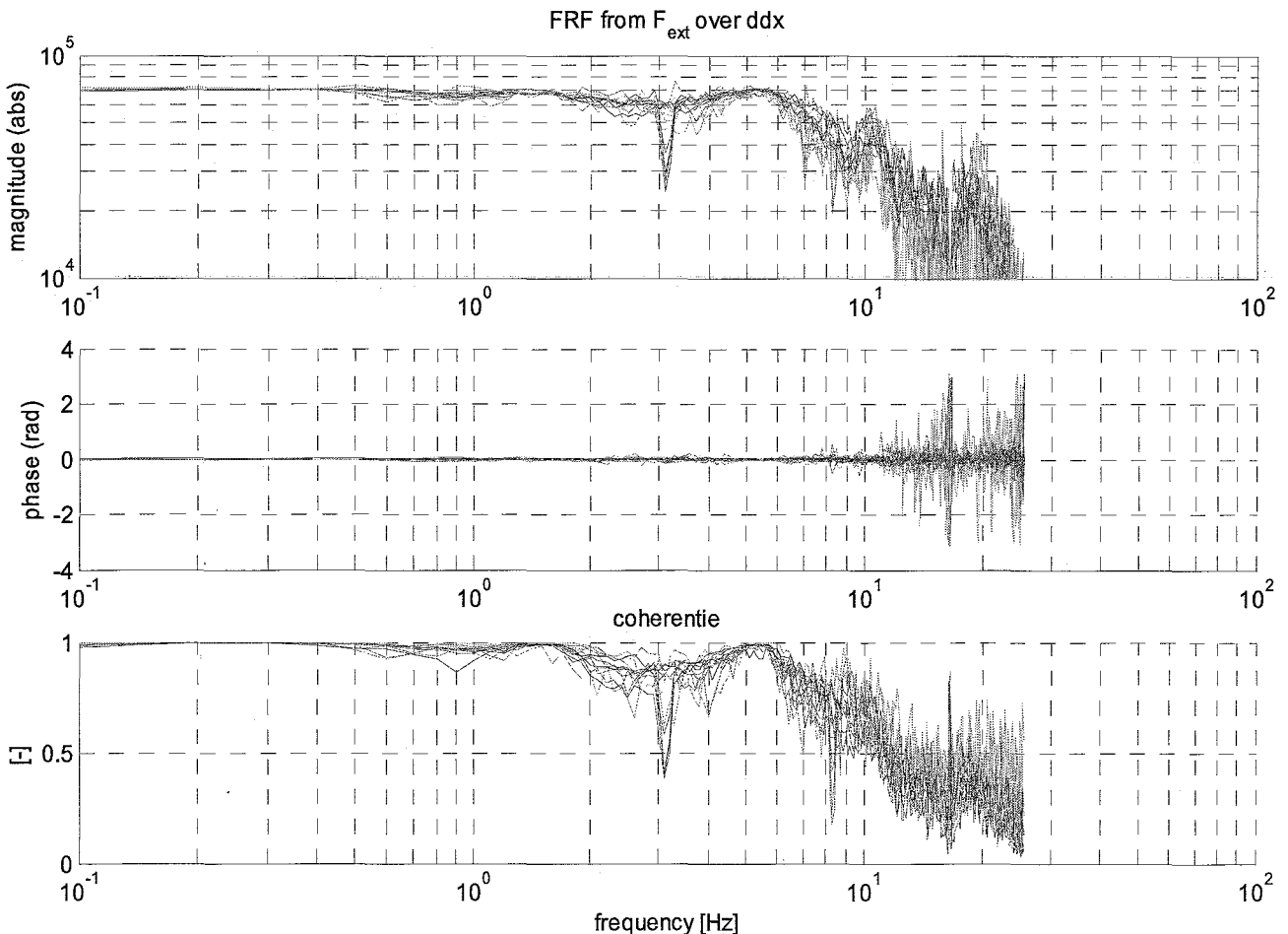


Figure 4.6 FRF and coherence of F_{ext} over \ddot{x}

$$\ddot{x}_{real} = \ddot{x}_{meas} - \frac{F_{ext}}{C} \quad (4.1)$$

The explanation for this is found in the torsion of the lock gate. When the cylinder extends, the fork clevis pulls on the topside of the gate. Since the water pushes in the opposite direction on the bottom side of the gate, a torsion moment is present in the gate. The lock gate is not infinitely stiff, and it will twist a little. The fork clevis will stand a little bit oblique, which causes the clevis to descend. Now the complete cylinder stands under an angle. The acceleration sensor, which was mounted on the clevis, will stand oblique and measure not only the acceleration in the axial direction, but also a part of gravity (fig 4.7 and 4.8).

If the piston is half in the cylinder, an angle of 1° of the fork clevis, gives a deflection of ca. 5.2 cm of the clevis. The piston will than stand under an angle of ca 0.54° . This means 0.95 % of the gravitational acceleration will be measured by the accelerometer ($= 0.091 \text{ m/s}^2$). This is a very large distortion compared to fig 4.4a.

The conclusion is that the accelerometer mainly measures the angle under which the cylinder stands, and not the axial acceleration. Since this angle is not constant, the measurement signal is much distorted.

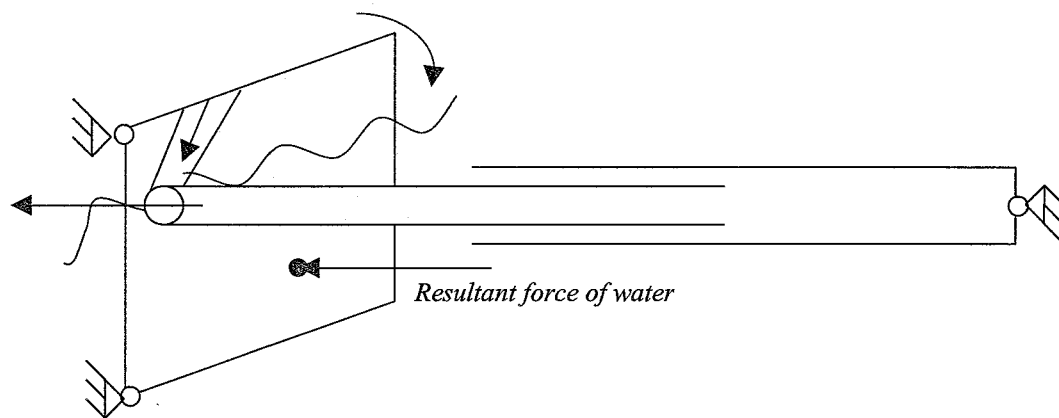


Figure 4.7 The pushing or pulling force of the cylinder, causes torsion of the lock gate, resulting in deflection of the fork clevis.

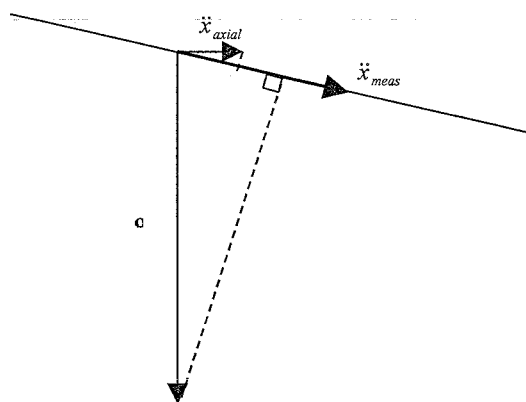


Figure 4.8 The effect of non-horizontal alignment of the accelerometer.

4.2.5 The strain gauge signal

DC offset

Since it was not possible to perform a zero calibration measurement for the strain gauge bridge (a measurement with zero force), the zero point of the strain gauge bridge had to be reconstructed from the measurements. Just as with the velocity measurements, the zero point changes over time. It is, however, not possible to determine a different zero point for each experiment, because not all

experiments have a reversal of movement. The ideal time to determine the zero point is at the reversal of the direction of movement. It appeared also possible to determine the zero point from the stop response in the outgoing movement.

The zero point used in the analysis was determined from the stop responses in the outgoing movement. A different zero point was determined for each velocity. It has to be mentioned, however, that the determined zero points are not very accurate.

Sensitivity

The sensitivity of the strain gauge amplifier was set on 0.23 mV/V. The equation for the conversion from bridge output to force is (app [B])

$$F = \frac{EA}{2(1+\nu)} \cdot \frac{4}{k} \cdot 10 \cdot Sen \cdot V \quad (4.2)$$

With an elastic modulus (E) of $208 \cdot 10^9$ (App [C]), a strain gauge factor (k) of 1.98, a sensitivity (Sen) of 0.23 mV/V, a Poisson's ratio (ν) of 0.3 and an output voltage of the strain gauge amplifier (V).

4.2.6 Pressure signals

DC offset

The conversion from milliampere to voltage gives a DC offset of 2 V. To determine the DC offset of the pressure transducers, a measurement was done when the pressure transducers were not connected to the hydraulic system. The atmospheric pressure is then measured. This measurement was used to correct for the DC offset of the pressure transducers.

Sensitivity

Since the pressure transducers are 400 bar pressure transducers with an output of 4-20 mA, which is converted to 2-10 V, the sensitivity is $50 \cdot 10^5$ Pa/V. The sensitivity has also been checked by accurate manometers with a lower maximum pressure (see app [D])

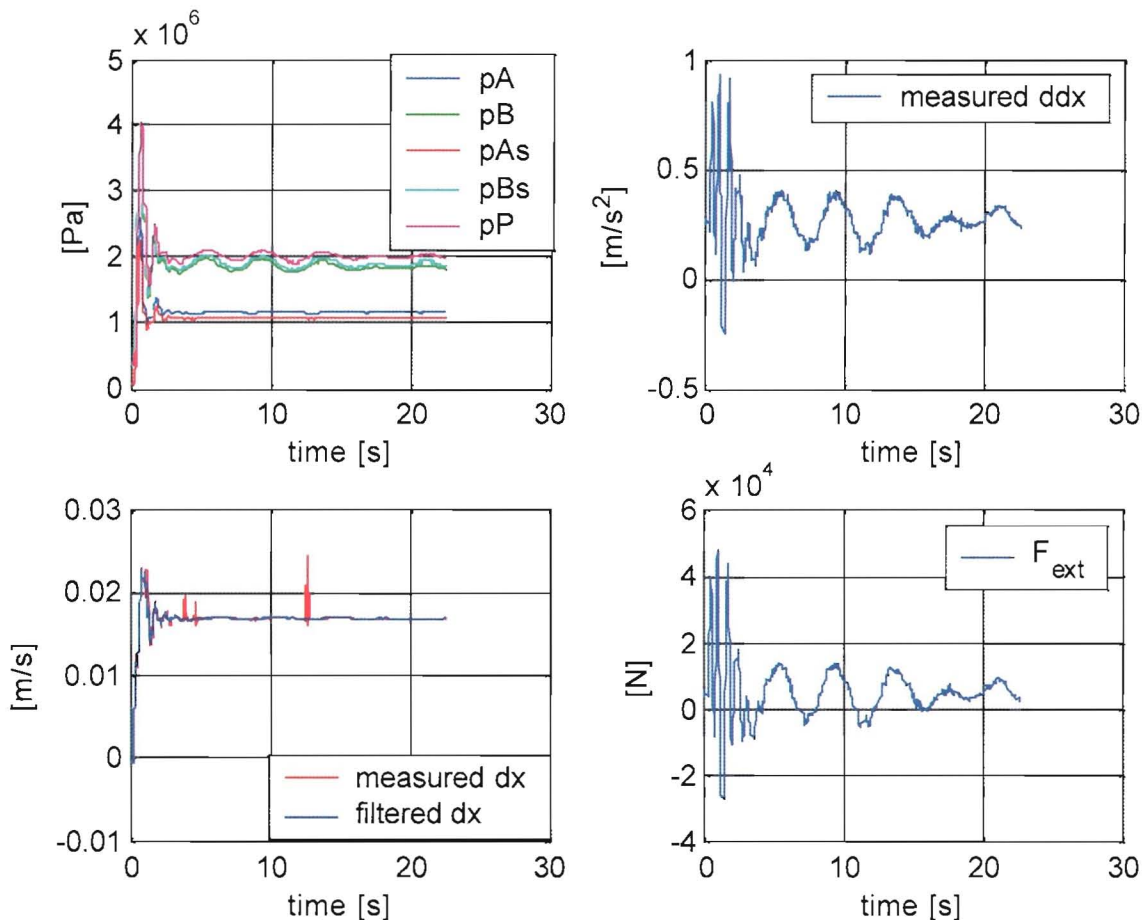


Figure 4.9 Example of measurement

$V_{control} = 5$ V, inward movement, position 2.4 m from clevis

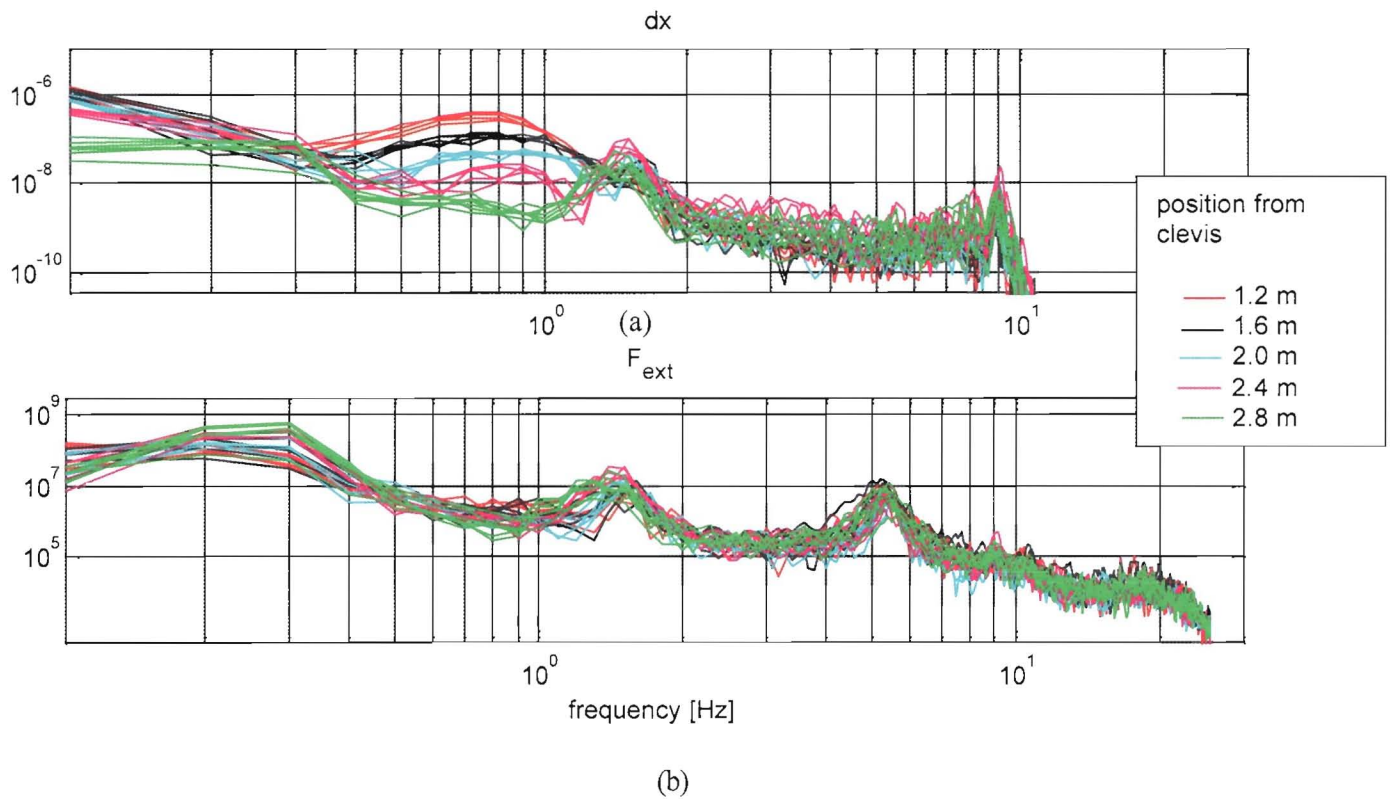


Figure 5.1 Power spectral density plots from (a) the velocity and (b) F_{ext}
 $V_{control} = 3 V$, inward movement

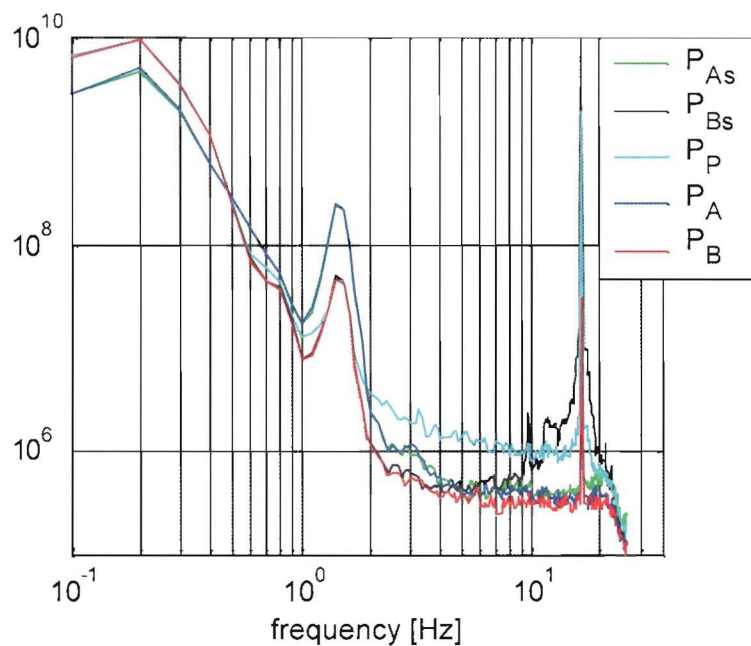


Figure 5.2 Power spectral density plot of the pressures.
 $V_{control} = 1 V$, position = 0.4 m, inward movement

Chapter 5: Results and identification

In this chapter the results and identification are described. First a frequency analysis is done to determine the important frequencies of the system. Next, the attempts to identify the parameters from the model of the hydraulic system are described. In paragraph 5.3 the friction is discussed and in paragraph 5.4 the behaviour of the driven system is discussed. At the end of each paragraph the conclusions are summarised.

5.1 Frequency analysis

The power spectral density (PSD) of a signal gives much information about the spectral contents. It shows the frequencies that are present in the data. The PSD can depend on position and velocity. It will also be different for the in- and outgoing movement. Figure 5.1 and 5.2 show examples of the PSD plots.

In the PSD's from all the data, a few frequencies are seen frequently.

- 17 Hz
This is the frequency of a complete round of the pump. It is seen very clear in the pump pressure and the pressure after the pump (p_{As} or p_{Bs}). In the other signals it appears as a very small peak, or not at all. In the external force and the filtered velocity, this frequency is filtered out.
- 5 Hz
This frequency is only seen in the external force measurements and the measurement of the acceleration. (Since it was established in paragraph 4.4 that the acceleration signal follows the force signal, the acceleration will be left out here.)
- around 1 Hz
This is a frequency, which is seen in almost all measurement with an ingoing movement. In the data from the outgoing movement this frequency is much less present. It is the frequency that is excited when the piston starts its movement and the static friction is overcome. At the outgoing movement, this frequency is much more damped than with the ingoing movement. The differential connection works as a damper. The frequency varies between ca 0.7 Hz and ca 1.5 Hz (fig 5.1a). It appears that a more outward position gives a higher frequency. This agrees with the theory about the natural frequency of the cylinder (see appendix A.4).
- around 0.2 Hz
For the lowest seen frequency, ca 0.2 Hz is difficult to find the exact frequency, because often the length of the data set is too short. It is a frequency found in almost all data, but mostly in the measurements with an outgoing movement. When the 1 Hz frequency is damped out, the 0.2 Hz frequency remains. It is only lightly damped.

5.2 Identification of the hydraulic system

The purpose of identifying the hydraulic system was to determine whether it can be neglected in the simulation model, and to find the parameter E . For this purpose, the hydraulic system was modelled (Chapter 1) as a series of volumes and resistance's.

Each volume is modelled as

$$\dot{p}_i = \frac{E}{V_i} (Q_{in} - Q_{out}) \quad (5.1)$$

$$Q_i = f(\Delta p_i, R_i) \quad (5.2)$$

To determine the different resistance's (R_i), volumes (V_i) and the bulk modulus (E), the time derivative of the pressure is needed. It is not measured, thus had to be calculated. It turned out to be impossible to identify the parameters of the model. In paragraph 5.2.2– 5.2.8, this is described.

5.2.1 Calculating the pressure time derivative

The time derivative is calculated by simply differentiating the pressure. Usually this is not a very good method, because noise on the pressure signal causes much larger noise in the time derivative of the pressure, especially with small sample periods.

In this case, the sample period will not be the problem (it is relatively large), but the resolution of the pressure signal can give a problem. For long periods of time, the pressure is almost constant and changes only one bit resolution at a time. These abrupt changes cause noise on the time derivative. To avoid this problem, the pressure signal is filtered with a low pass filter, which rolls off steep at 10 Hz. This seems a low frequency, but the only frequency higher in the signal is 17 Hz, from the pump. Figure 5.3 gives an example of a time derivative.

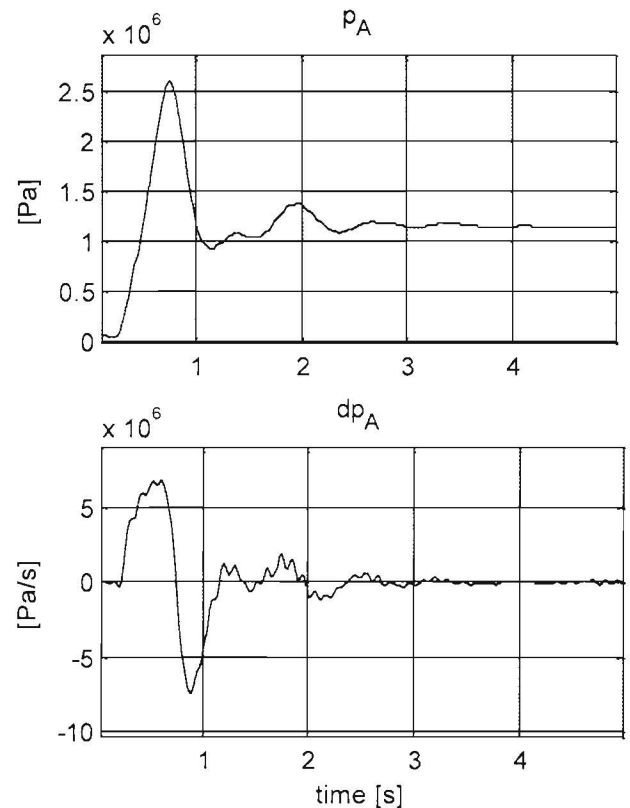


Figure 5.3 Example of a time derivative of the pressure.

5.2.2 Calculating R_x from the stationary state

The most obvious way to calculate the resistance parameters is from the stationary state. If

$\dot{p} = 0$, the ingoing flow equals the outgoing flow (eq (5.1)) and the pressure equations of the model (fig 1.9 or 1.10) can be filled out because there are 5 equations and 5 unknown parameters (4 resistance's and the flow from the pump Q_m). However, the limitation is that only a pure linear or pure quadratic model can be used. Since it is not likely that the system is purely linear or quadratic, this method will not give correct results. If the calculated R_x is plotted against the calculated flow, this should produce a straight line. It does not (fig 5.4)

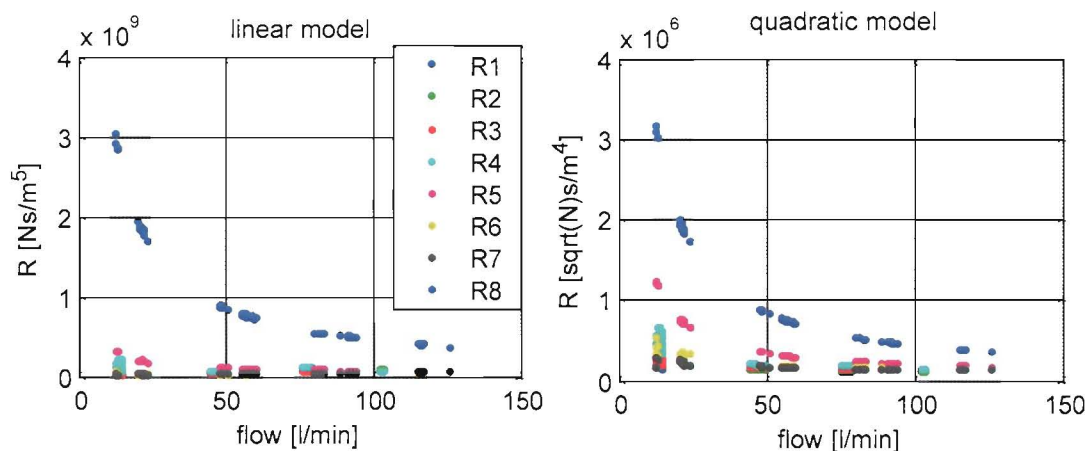


Figure 5.4 Calculated resistance's with a (a) linear and a (b) quadratic model. The resistance's are defined according to fig 1.9 and 1.10.

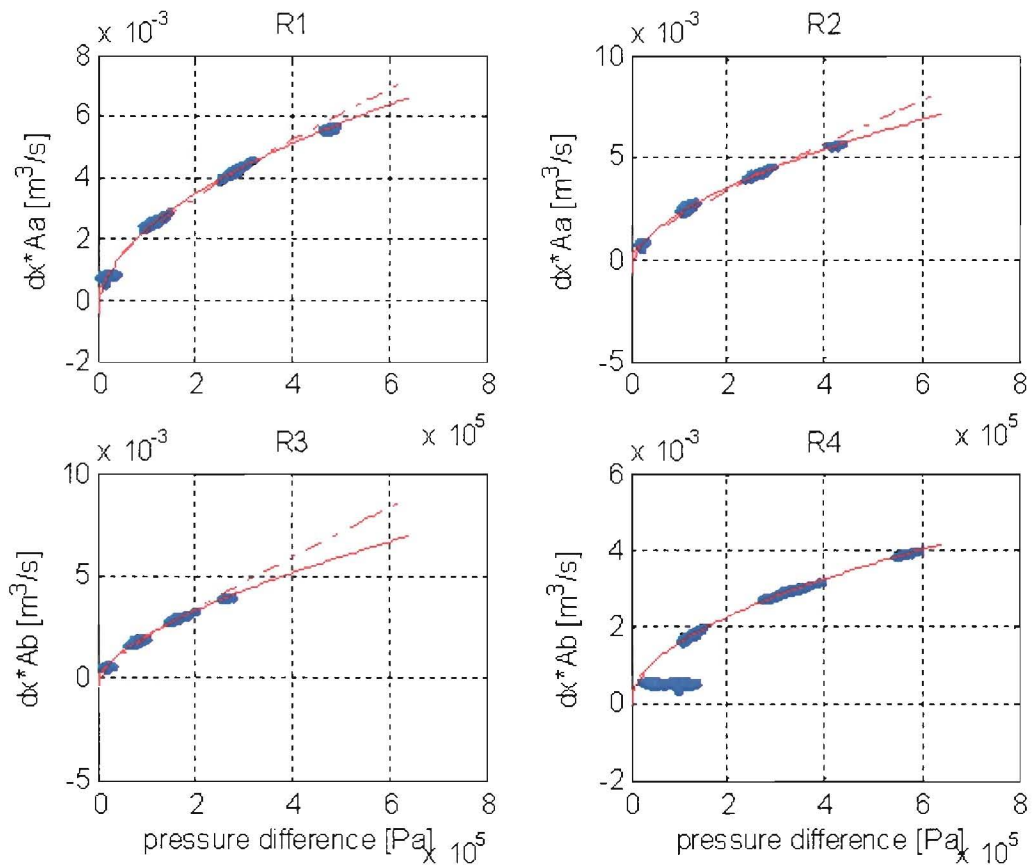


Figure 5.5 Functions $Q_i = f(\Delta p_i, R_i)$ for the outgoing movement. On the horizontal axis the pressure difference for the appropriate resistance (see fig 1.10) and on the vertical axis the flow calculated from the velocity of the piston and the appropriate area.

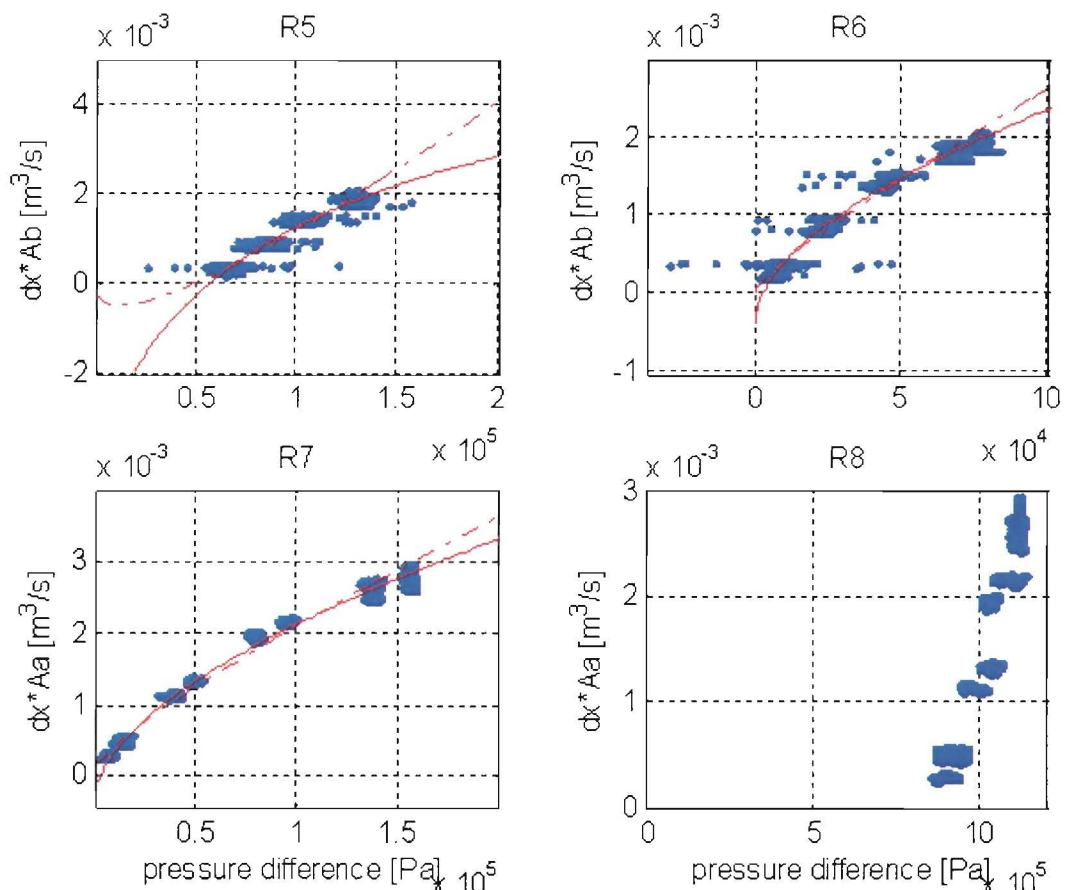


Figure 5.6 Functions $Q_i = f(\Delta p_i, R_i)$ for the ingoing movement. On the horizontal axis the pressure difference for the appropriate resistance (see fig 1.9) and on the vertical axis the flow calculated from the velocity of the piston and the appropriate area.

5.2.3 Calculating the function $Q_i = f(\Delta p_i, R_i)$

A way to include the linear and quadratic approach in one model is to plot the flow against Δp and fit a model. This is done with all measurement points, except the first 4 seconds of the start and stop response. After these first 4 seconds, the flow is assumed to be constant. The flow is then calculated from the velocity and area of the piston. Since \dot{p} is not equal to 0, an error is made. This is however a small error and will not effect the results much.

The results can be seen in fig 5.5 and 5.6. The equation fitted trough the data is equation (5.3).

$$Q_i = \frac{\Delta p_i}{R_{i,l}} + \frac{\sqrt{\Delta p_i}}{R_{i,q}} + C \quad (5.3)$$

The solid line is the best fit for ($C = \text{Constant}$), the dotted line is the best fit for $C = 0$. The assumption $C = 0$ seems more realistic, because when there is no pressure drop, there is no flow. It, on the contrary, is possible the have a pressure drop and no flow, for instance with preloaded check valves. The resistance's with an in going movement of the cylinder (differential) look quite good, except R4 at the lowest flow. Since R2 and R3 are physically equal to R7 and R6, these plots should be equal and so they are.

In the model, it is assumed that the pressure in the tank is atmospheric pressure. This calculation predicts a pressure of ca 8.5 bar in the tank. A partial explanation comes from the return filter before the tank. Next to the filter is a preloaded check valve, which opens when the filter is clogged. However, the instruction book [Rex01] of the lock specifies that the check valve opens at 3.5 bar, not at 8.5 bar.

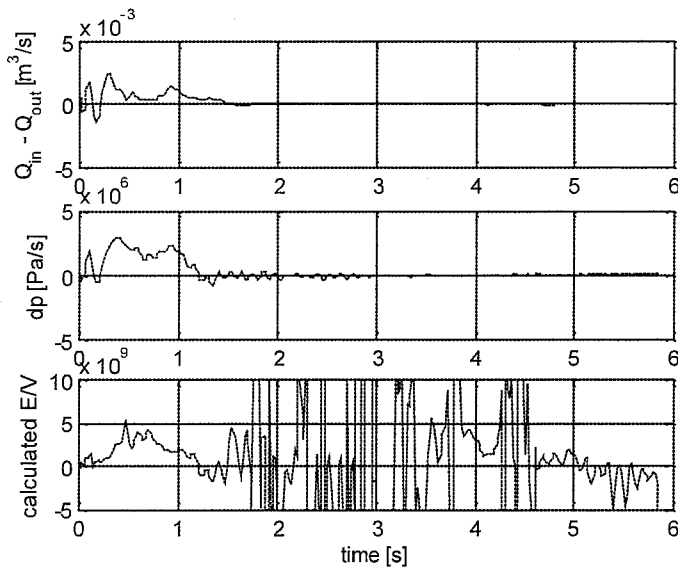


Figure 5.7 Results from calculating E/V of the bottom side of the cylinder from $Q = f(\Delta p, R_x)$.

(a) $Q_{in} - Q_{out} [m^3/s]$ (b) $\dot{p} [Pa/s]$ (c) E/V

5.2.4 Calculation $\frac{E}{V_i}$ from $Q_i = f(\Delta p_i, R_i)$

The parameters E and V_i in eq (5.1) cannot be estimated separately, so the quotient $\frac{E}{V_i}$ is estimated.

In paragraph 5.2.3, a function $Q_i = f(\Delta p_i, R_i)$ is found. This function is used to find

$$\frac{\dot{p}_i}{Q_{in} - Q_{out}} = \frac{E}{V_i} \quad (5.4)$$

Results as plotted in figure 5.7 are found. Figure 5.7 plots \dot{p} and $Q_{in} - Q_{out}$, and the quotient of both. The estimated $\frac{E}{V_i}$ is not constant and it is not possible to determine a suitable $\frac{E}{V_i}$. A constant $\frac{E}{V_i}$ cannot be expected from these measurements, because the time derivative of the pressure and the net flow are not shaped alike. A constant quotient can not be found.

5.2.5 Estimating $\frac{E}{V_i R_i}$ with a least squares estimate

A last attempt made to find the parameters E , V_i and R_i is the estimation of $\frac{E}{VR_i}$ with a least squares estimation. Equation (5.1) with a combination of a linear and quadratic flow model can also be written as equation (5.5) in the hydraulic system or equation (5.6) for the pressure in the bottom side of the cylinder.

$$\dot{p} = \frac{E}{V_i} \left(\frac{\Delta p_{in}}{R_{in,l}} + \frac{\sqrt{\Delta p_{in}}}{R_{in,q}} - \left(\frac{\Delta p_{out}}{R_{out,l}} + \frac{\sqrt{\Delta p_{out}}}{R_{out,q}} \right) \right) \quad (5.5)$$

$$\dot{p} = \frac{E}{V_i} \left(\frac{\Delta p_{in}}{R_{in,l}} + \frac{\sqrt{\Delta p_{in}}}{R_{in,q}} - \ddot{x} \cdot A_A \right) \quad (5.6)$$

With these equations, the parameters $\frac{E}{VR_i}$ were estimated. As can be expected from figure (5.7), it makes a large difference which part of the data is used for the estimation.

An example of the results is figure (5.8 (a,b)). The estimation is based on the time interval 0.6-4 seconds. If the lines for the real and estimated \dot{p} are compared, the estimation looks good. However, the lines for $E/V \cdot Q$ indicate for the annular side (b) either a negative flow, or a negative volume or bulk modulus. The flow is not negative (the cylinder would than move the other way) and the bulk modulus and volume cannot be negative. This is not a correct solution. For a lot of the data, similar conclusions had to be drawn.

Some sources of error can be found by looking at figure 5.8c, which shows the used time measurement:

- The pump pressure first drops and takes half a second to regain its position in the middle of the five pressure signals. Even though the pump pressure is lower than the pressure in the base and piston side of the system, they both rise. An explanation for this was not found.
- The pressures in the beginning of the rising of the pressure are so close together that a measurement error would have enormous effect on the estimation.

Also the volume (V) in the estimation changes during the estimation. In the 3.6 seconds involved in the estimation, the volume on the base side changes ca 8%. For a measurement at the end or beginning of the stroke, this relative change would be much larger.

Not only this gives strange results. Also the estimates of the pressure in the bottom and annular side of the cylinder show strange results. Almost all of the estimation sets of the pressure parameters were physically impossible for one of the following reasons:

- The direction of the flow was wrong.
- The parameter E/V found for the pressure in the cylinder on side A or B was too low (for example 5000, while an E/V of ca $1 \text{e}8\text{-}1 \text{e}9$ was expected).

No complete set of physically possible solutions was found.

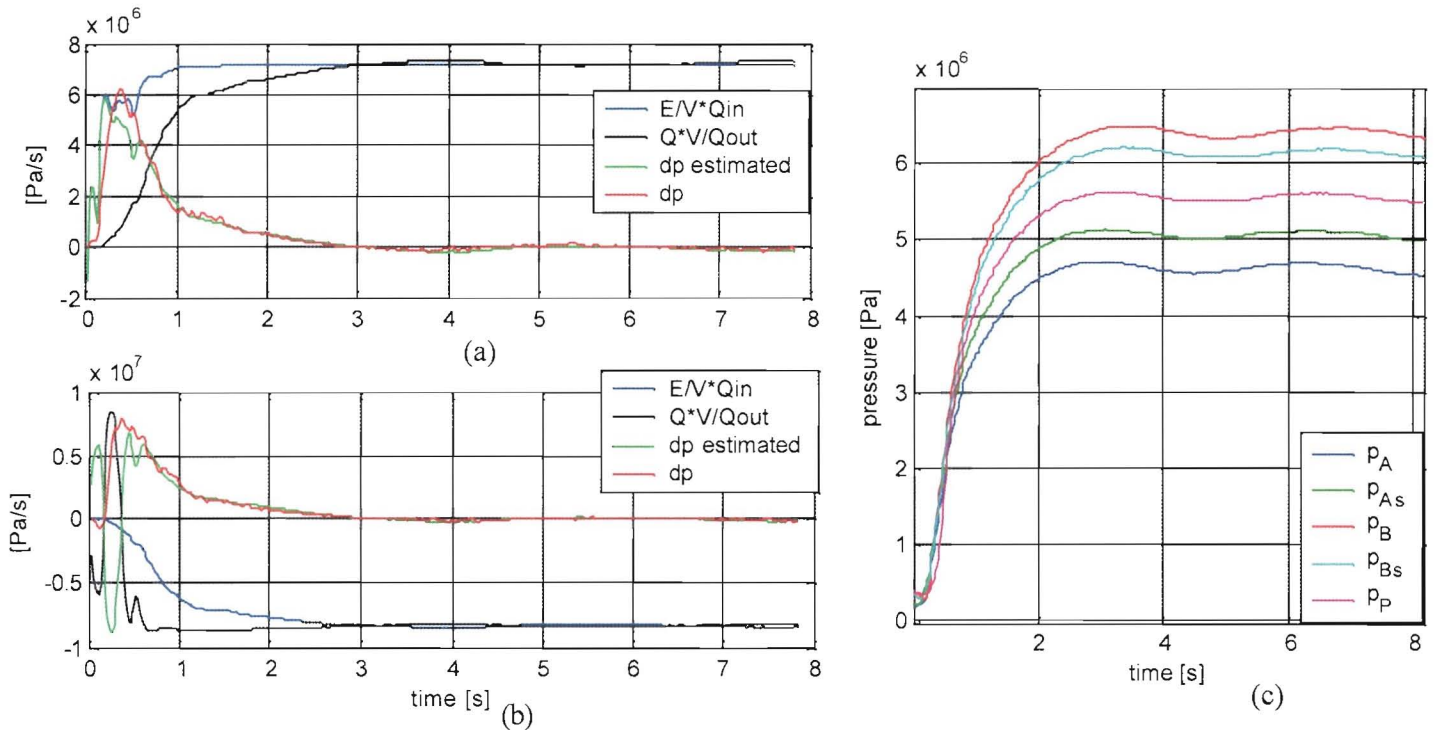


Figure 5.8 (a) Example of results of an estimation of E/VR in the cylinder on (a) bottom side and (b) annular side, and (c) time measurements of pressures of the measurement

Estimated values A: $E/V = 1.28 \cdot 10^9$, $E/VR_{in,l} = -16.2$, $E/VR_{in,q} = 2.2 \cdot 10^4$
 B: $E/V = -2.1 \cdot 10^9$, $E/VR_{out,l} = 45$, $E/VR_{out,q} = -3.9 \cdot 10^4$

$V_{control} = 7 \text{ V}$, position = 2.8 m, outward movement

5.2.6 The effect of model and measurement errors

The effect of an offset in Δp

Since it is not known exactly how long SigLab was on when the zero point measurement for the pressure was done, it is possible that there is an extra dc offset present (see appendix [D]). An extra DC offset of 4 mV would give an error of 0.2 bar, which is substantial in the low-pressure differences present. In figure 5.8c, an example of the pressure differences from an outward movement can be seen. In the inward movement, the pressure difference between the pump pressure and the pressure on the annular side of the hydraulic system and the difference between the pressure on the annular side of the cylinder and the pressure on the annular side of the hydraulic system are even lower. Pressures below 1 bar and even below 0.5 bar in stationary state were measured.

Pressure dependent bulk modulus

In appendix A.1, it is explained that the bulk modulus depends, among others, on the pressure, especially for low pressure ($< 60 \text{ bar}$), which is the work range for the cylinder. A pressure drop of 10 bar can halve the bulk modulus.

Neglected inertia of the fluid

The inertia of the fluid is not taken into account in the model. A quick estimation of the pressure drop from inertia is

$$F = m\ddot{x} \quad (5.7)$$

$$\Delta p A_{tube} = \rho V \frac{\dot{Q}}{A_{tube}} \quad (5.8)$$

$$\Delta p_{inertia} = \frac{\rho L A_A \ddot{x}}{A_{tube}} \quad (5.9)$$

For a 5 m tube of diameter 30 mm, this would give a pressure drop of $4 \cdot 10^4 \cdot \ddot{x}$. With a maximum acceleration for start responses of ca 1 m/s^2 , this can give a pressure loss of 0.4 bar. Which is substantial, compared to the pressure drops measured.

5.2.8 Conclusion

Practically, the pressure losses are used as flow meters for identification. Inaccuracy's in the pressure measurement, and neglect of the inertia of the oil gives deviations in the flow characteristics (fig 5.5 and 5.6), which makes it impossible to identify the hydraulic system and pressure dynamics of the cylinder this way. Since the flow is used as a criteria for neglecting the hydraulic system (if the flow from the pump into the system is the same as the flow from the system into the cylinder, the hydraulic system can be neglected), no conclusions can be drawn on this subject.

5.3 Friction

5.3.1 Calculation of friction

The friction in the cylinder is calculated from (see eq 2.1)

$$F_w = pA \cdot A_A - pB \cdot A_B + F_{ext} \quad (5.10)$$

The influence of the inertia force $M\ddot{y}$ (M is the mass of the rod group and oil) is neglected, since it is much smaller than the other forces.

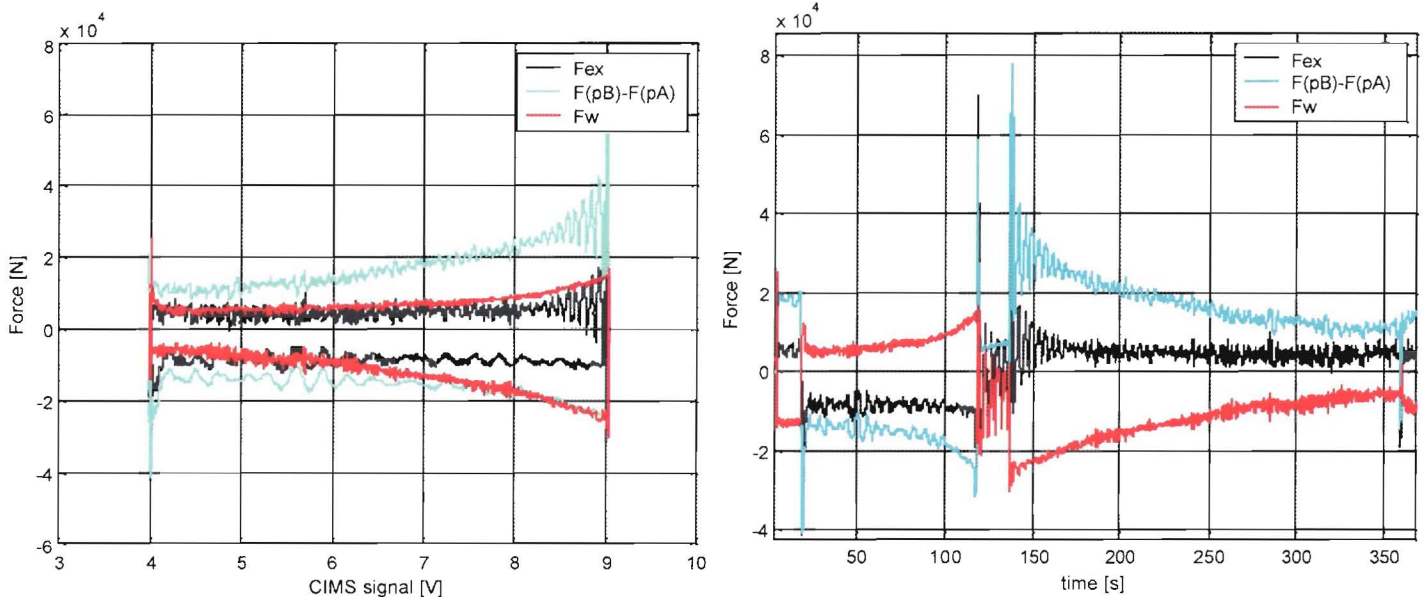


Figure 5.9 Forces on the piston (a) position dependent (b) time dependent [N]

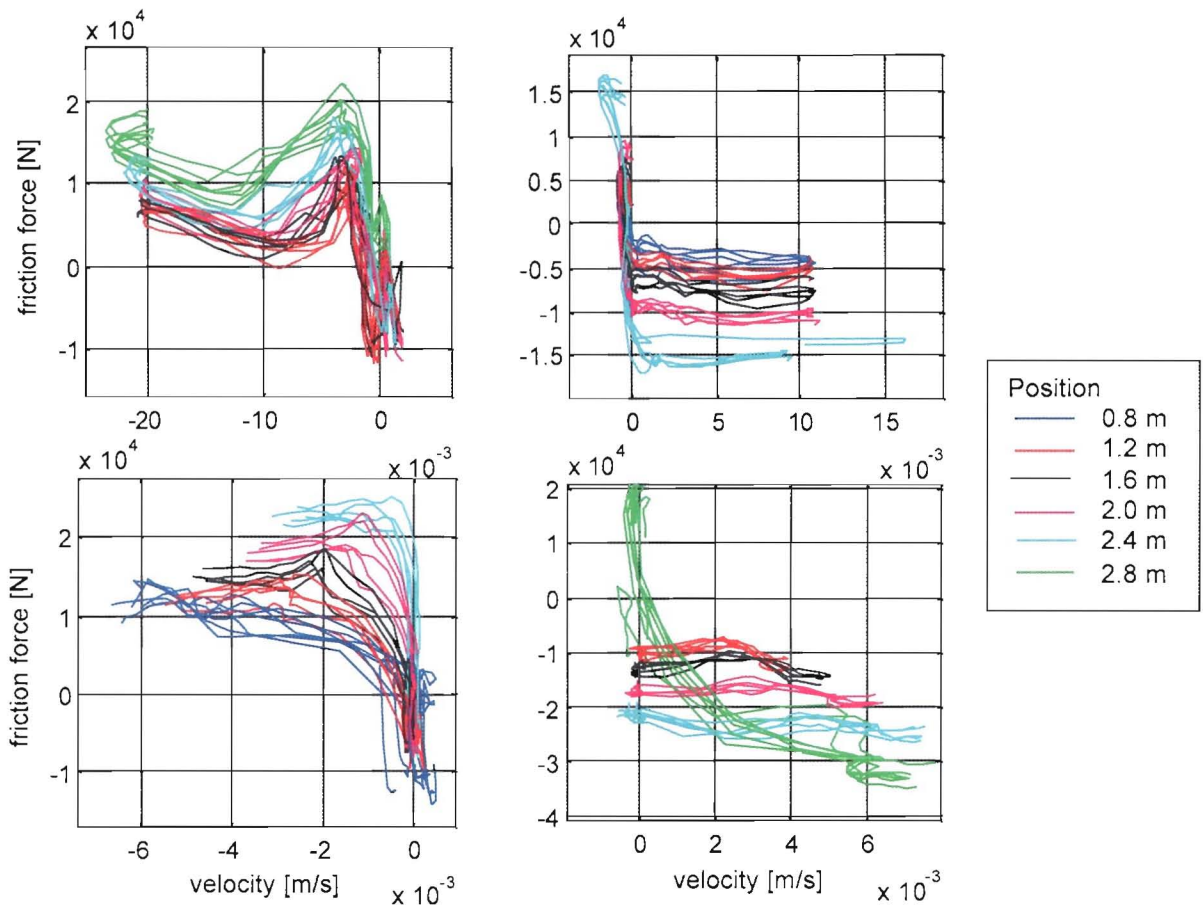


Figure 5.10 Position dependence of friction curves of (a) inward stop response (b) outward stop response (c) inward start response (d) outward start response

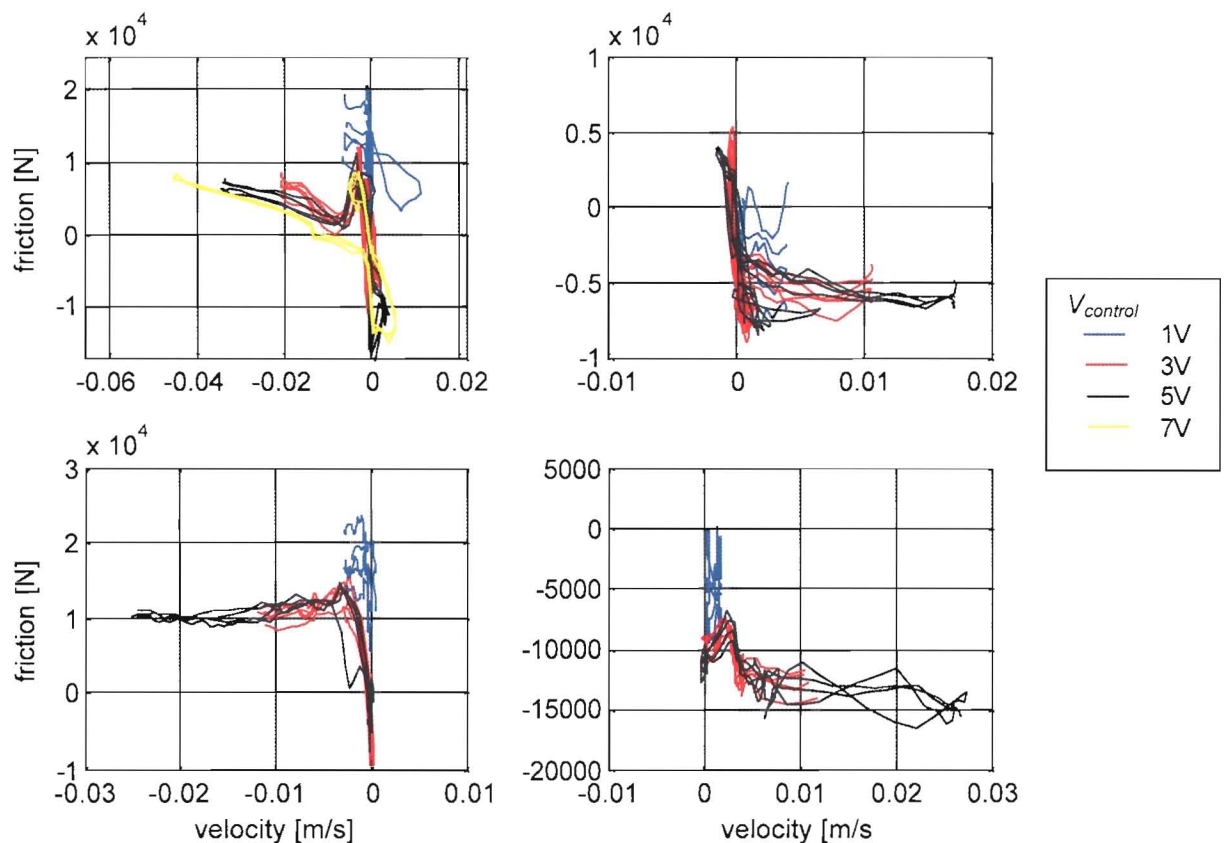


Figure 5.11 Velocity dependence of friction curves of (a) inward stop response (b) outward stop response (c) inward start response (d) outward start response
Control signal: blue: 1 V, red: 3 V, black: 5 V, yellow: 7 V

Figure (5.9a) gives an idea of the magnitude of the forces.

In figure (5.9b) the friction force for the same experiment as a result of the position is drawn. Here, it is concluded that the friction force increases when the cylinder is extended. A bending moment will be present in the rod due to its own weight. This bending moment has to be transferred from the rod to the shell group via the bearing strips in the piston and the cylinder head. When the cylinder extends, the distance between the piston and the head decreases, resulting in higher bearing loads and higher friction.

5.3.2 The Stribeck curve

When the friction force is plotted against the velocity during start and stop, a Stribeck curve as depicted in figure (1.7) is expected. As was established in paragraph 5.3.1, a dependence on the position will be present. Also, a dependence on the direction of movement is seen (see fig (5.10)). The dependence on position is obvious: a more outward position gives more friction, as was also seen in figure (5.9). Furthermore, it is noticed that in the inward movement no peak in the friction for low velocities is present. This difference can be explained by the fact the seals and bearings on the cylinder head slide over a dryer surface in the outward movement, which gives more friction than the inward movement, where the seals slide over an oiled surface. The peak is caused by dry friction.

The start responses also show different behaviour than the stop responses. Generally, the start response shows more friction than a stop response.

Figure 5.10 and 5.11 make it clear that only simple Stribeck curve does not describe the friction very well. In the literature, models can be found, which explain more of the phenomena seen in figure 5.10 and 5.11. For instance the LuGre friction model. More about friction can be read in [Ibr92].

5.3.3 Conclusion

The magnitude of the friction force is of the same order as the other forces on the rod. With a constant velocity, the friction is dependent on the position of the piston and very reproducible. The Stribeck curves are dependent on the direction of movement, the position, the value and sign of the acceleration and also quite reproducible. More complicated models than the Stribeck curve are necessary to describe the dynamic friction behaviour.

5.4 Identification of load dynamics

The purpose of identifying the load dynamics is to find a way to calculate the external force in the simulation model. The external force could be a function of position, velocity and acceleration. An easy way to implement such a calculation in the simulation model is by way of a FRF. Another way could be via characteristic curve, which can depend on position and velocity.

In paragraph 5.4.1, an attempt is made to find an FRF, in paragraph 5.4.2, a characteristic curve is discussed.

5.4.1 Frequency Response Function

When the load dynamics would be linear, they could be described with a FRF. Since the acceleration signal was not correct, a FRF of F_{ext} over \dot{x} is drawn in figure (5.12). As can be seen, the coherence (fig 5.12c) is low: the FRF is not accurate. This has multiple reasons. Firstly, the transfer is probably non-linear and more important, secondly, there only is energy content on a few frequencies. FRF 's of frequencies that are not present in the signals cannot be determined. In figure 5.13 can be seen that only a few frequencies are present in the data. Low coherence was found in all FRF's of F_{ext} over \dot{x} , mostly lower than in figure (5.12c). Since the coherence between F_{ext} and \dot{x} is low, the coherence between F_{ext} and \ddot{x} will be low too.

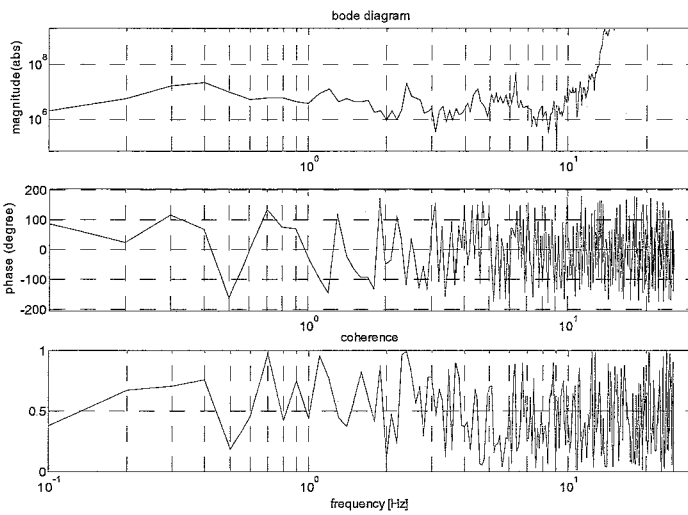


Figure 5.12 FRF and coherence of \dot{x} over F_{ext}

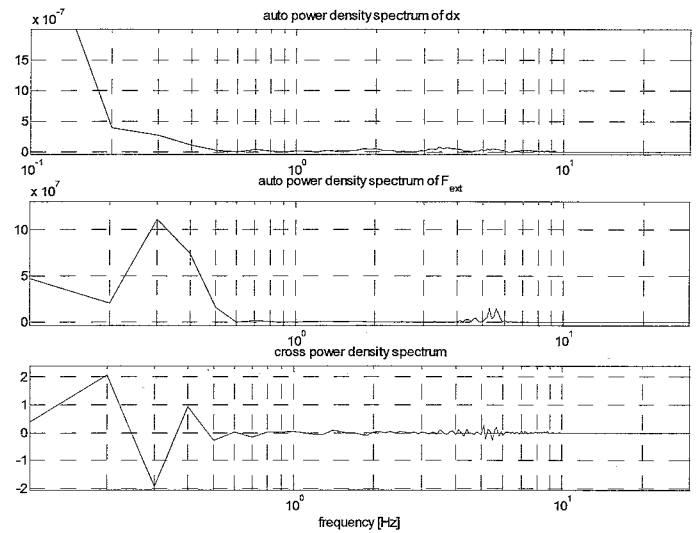


Figure 5.13 Power density spectra

5.4.2 Load characteristic

The external force on the rod is expected to consist of the friction in the hinges, the inertia of the gate and the moving water, and the resistance of the water to the movement of the gate. This resistance probably depends on the position of the gate (close to the wall, or far from the wall).

Figure 5.14 shows a plot of F_{ext} as a result of the velocity of the piston. It is drawn from the measurements between $t = 4$ s and the end of the measurement. In these data, the acceleration was almost zero, which would exclude effects of inertia. The shape of the curve looks very illogical. For positive velocities, a larger velocity means less force, for negative velocities, a larger velocity means more force. When the magnitude of F_{ext} is viewed and compared to the zero point shift of the strain gauge bridge, it can be concluded that it is very well possible that the shape of the characteristic curve in figure 5.14 is a result of zero point shift of the strain gauge bridge and thus figure 5.14 can not be used for the simulation model.

5.4.3 Conclusion

A way to calculate the external force on the piston could not be found. This was among others due to the limited amount of frequencies in the signals and the large zero point drift of the strain gauge bridge.

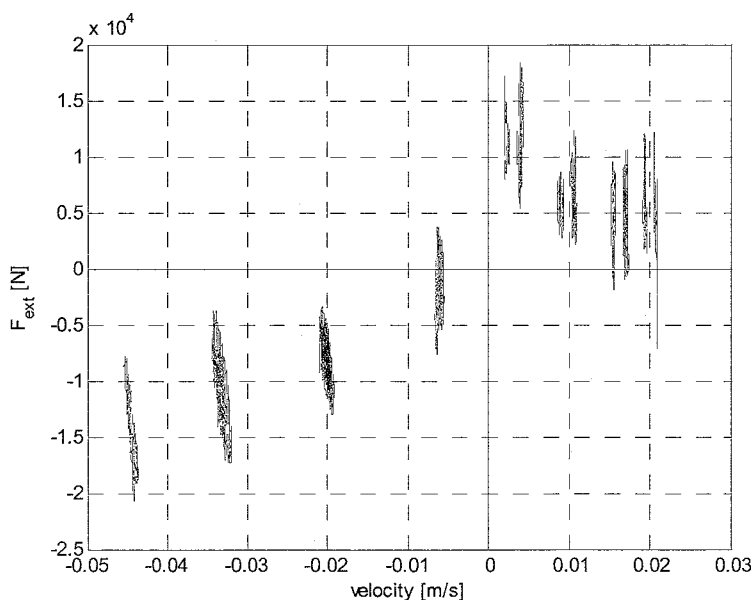


Figure 5.14 Relation between velocity and F_{ext}

Chapter 6 Conclusions and recommendations

The objective of this report was to validate the simulation model, which was constructed in the 'Friction Induced Vibrations' project. For this purpose, measurements were done on a cylinder of a lock. With the data from these measurements an attempt was made to find the parameters from the model. This turned out to be very difficult, due to measurement errors and model errors. In the paragraphs below the conclusions and recommendations about measurements, identification and the simulation model are given.

6.1 Measurements

The main problems with the measurements were caused by the fact that the measured quantities were very small. Because these quantities were so low, zero point drift of the data-acquisition system and the sensors had a large effect on the measurements. Especially because the measurements often showed a DC offset, which was not constant and thus not accurately corrected for. Part of these problems can be resolved by using different sensors, with a range that is better suited for the range of the measured data. For instance, if 100 bar pressure transducers would be used instead of 400 bar pressure transducers, the measurement error due to dc drift would be 4 times lower. Another way to increase the accuracy of the measurement is to use a circuit to convert the milliAmpere signals to a ± 10 Volt signal, instead of a 500 Ohm resistance, which converts the ampere signals to a 2 – 10 Volt signal.

The signals then have a lower DC offset, which make it possible to measure with a smaller resolution. This can also be achieved by measuring the signals with respect to a stable offset voltage.

To minimise zero point drift in the data-acquisition system and possibly other measurement devices, it is necessary to use a large warming up period.

Another problem was the large distortion of the acceleration signal. The finite stiffness of the lock gate caused the fork clevis to deflect. The resulting angle variations of the clevis caused the accelerometer to measure under different angles from the horizontal plane. The gravitational acceleration gave a large distortion of the acceleration signal, which made it unusable for the identification. This is a problem that can be solved by using a tri-axial accelerometer.

Measuring the position and velocity with CIMS is in principle possible. The present available signal is not accurate, but the nonlinearity's can be compensated and the resolution increased when the digital pulses are measured. For this use, a measurement system for simultaneous sampling of the counter values and the analogue signals has to be developed and research has to be done for correction the periodic (10 mm) non-linearity of the CIMS signal.

6.2 Identification

Good identification of the steady state values is possible. The resistance's of the hydraulic system were identified and the friction (dependence on the position) is very reproducible.

It was not possible to identify the dynamic parameters from the model of the hydraulic system. The used model does not approach reality and therefore identification can lead to physically impossible parameters or not identifiable parameters. Including inertia effects in the pipes in the model, could perhaps give a better representation of reality. Since the flow cannot be determined accurately, no conclusions can be drawn about whether it is possible to neglect the hydraulic system.

For the start and stop responses, Stribeck curves could be drawn that are reproducible. However, the curve is very dependent on the direction of movement, position, and the value and sign of the acceleration. It is not possible to find a Stribeck curve that can easily be used in the simulation model. Friction is a highly non-linear phenomenon that is largely dependent on many factors. The steady state Stribeck curves that are measured do not represent friction in dynamic situations well.

It was not possible to find an easy description of the dynamic behaviour of the lock gate. This was due to likely non-linear behaviour, small frequency content of the signals and zero point shift of the strain gauge bridge signal.

6.3 Validation

Since it was not possible to identify the parameters of the model, it is not possible to validate the model. However, since the conclusion was drawn that the friction of the cylinder could not be captured in a single or a small set of Stribeck curves, and stick-slip vibrations originate from friction for low velocity's, the question will have to be raised whether it is possible to accurately predict stick-slip with the simulation model. Possibly it is possible to determine a 'worst case scenario' and use this in the prediction model.

Bibliography

- [Den98] Denbigh, P., "Systems Analysis & Signal Processing", Addison Wesley Longman Ltd (1998)
- [Gel74] Gelb, A. e.a., "Applied optimal estimation", The M.I.T. Press (1974)
- [Jel03] Jelali, M., Kroll, A., "Hydraulic Servo-systems, Modelling, Identification and Control", Springer-Verlag London Berlin Heidelberg (2003)
- [Fen93] Fenner, Roger T., "Mechanics of Solids", CRC Press (1993)
- [Fig00] Figliola, Richard S., Beasley, Donald E., "Theory and Design for Mechanical Measurements", third edition, John Wiley & Sons, Inc. (2000)
- [Gra93] Graham Kelly, S., "Fundamentals of mechanical vibrations", McGraw-Hill Book (1993)
- [HBM] HBM, "Strain gauges and accessories"
- [Hof89] Hoffmann, K., "An Introduction to Measurements using Strain Gages", Hottinger Baldwin Messtechnik GmbH, Darmstadt (1989)
- [Hydac] Hydac electronic, specifications pressure transmitter HDA 4400/HDA 4700
- [Ibr92] Ibrahim, R.A., Soom, A., ed. "Friction-induced vibration, chatter, squeal, and chaos", The American society of mechanical engineers (1992), Symposium reports
- [Keller] Keller, piezoresistive pressure transmitters, specifications, from www.keller-druck.com
- [Kui99] Kuijpers, M.R.J., "Modelling and identification of a one-mass system with friction", master thesis TU Eindhoven (1999)
- [Mantra] Mantracourt, "SGA/A & SGS/D strain gauge transducer amplifier, user manual instructions"
- [Poly03] Leijendeckers, P.H.H. et al, "Polytechnisch zakboek" 49^e ed., Elsevier bedrijfsinformatie bv (2003), in Dutch
- [Rex01] "Instructieboek tbv renovatie oranje sluizen zuidersluis schellingwoude" Book 1 & 2, project nr. 961448 Rexroth B.V. (2001), in Dutch
- [Rex03] Molenaar, M., "friction induces vibrations", Rexroth-Hydraudyne, (2002)
- [Rij03] Rijswick, R.J.A., "Friction induced vibrations in hydraulic cylinders", Master thesis TU Eindhoven (2003)
- [Vie90] Viersma, T.J., "Analysis, Synthesis and Design of Hydraulic Servosystems and Pipelines", TU Delft (1990)

Appendix A Theory of the model

Appendix A.1 Effective Bulk Modulus

The bulk modulus of a fluid is the modulus of elasticity of a fluid. It is defined as

$$E \equiv \rho_0 \left(\frac{\partial p}{\partial \rho} \right)_\theta = -V_0 \left(\frac{\partial p}{\partial V} \right)_\theta \quad (\text{A.1})$$

where θ stands for constant temperature.

The effective bulk modulus (E) is influenced by the volume of gas entrained in the fluid, pressure, temperature and mechanical compliance of the (for instance) pipelines. Figure A.1 shows the effect of entrained gas. Table A.1 shows some experimental results on the effect of mechanical compliance on the effective bulk modulus.

For mineral oils, a typical bulk modulus is $1.4\text{-}1.6 \times 10^9$ Pa. However, the effects of entrained air and mechanical compliance can lower the effective bulk modulus to 10% of this value [Vie90], especially at low pressures (fig A.1). More detailed information on effective bulk modulus can be found in [Jel03].

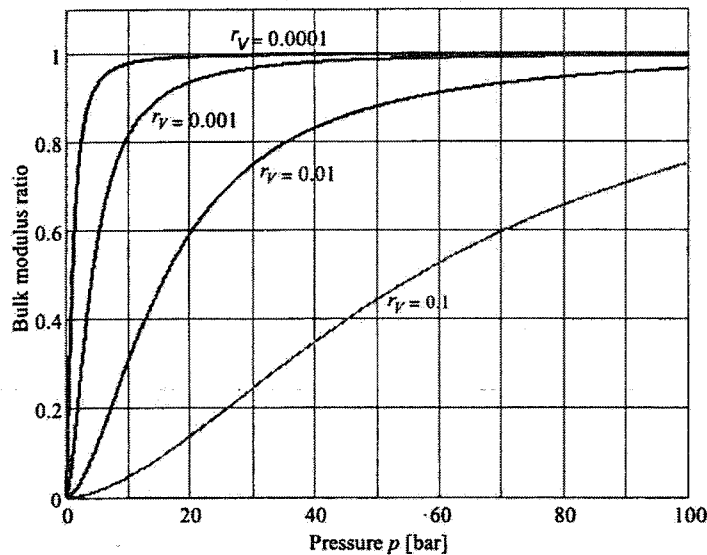


Figure A.1 Influence of entrained air volume on the effective bulk modulus. Bulk modulus ratio is $E(\text{entrained air}) / E(\text{no entrained air})$, r_v is $V_{\text{gas}} / V_{\text{liquid}}$ [Jel03]

Nominal pressure [MPa]	E [MPa] for steel pipeline $R_i = 6.25$ mm; $R_o = 8$ mm	E [MPa] for high-pressure Hose $R_i = 6.25$ mm
5	1460	500
9	1510	537
13	1570	568
22.5	1890	

Table A.1: Values for bulk modulus E [Jel03]

Appendix A.2 Added Mass

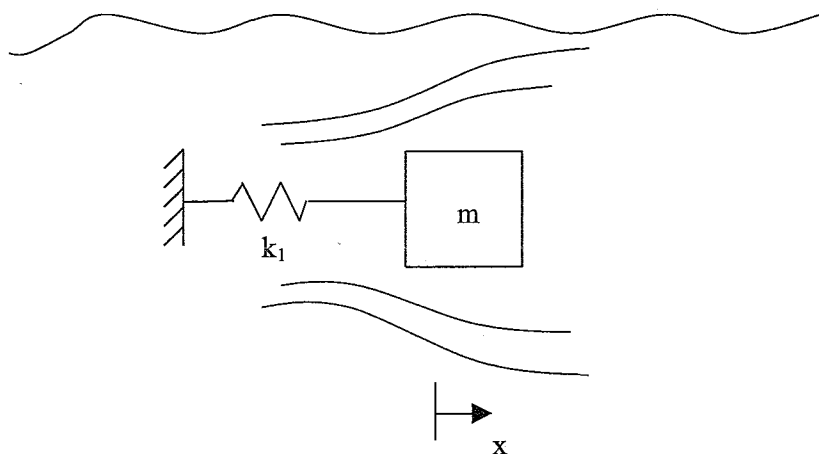


Figure A.2 Mass-Spring system in a fluid

[Gra93] If an object is moved through a fluid, it feels an extra mass, besides the mass of the object. This mass (added mass) can be calculated from the energy equation.

$$T_m + T_f + V = C \quad (\text{A.1})$$

Here, T_m is the kinetic energy of the object, T_f is the kinetic energy of the moving fluid, V is the potential energy and C is a constant.

The kinetic energy of the fluid is not easy to determine. From potential flow theory, the velocity distribution of in a fluid for a body with constant velocity can be calculated [Gra93]. Integrating the squared velocity distribution gives the kinetic energy (eq (A.2))

$$T_f = \frac{1}{2} \iiint \rho v^2 dV \quad (\text{A.2})$$

Since the lock gate rotates around a fixed axis, not the added mass, but the added moment of inertia is the parameter of interest.

$$I_a = \frac{T_f}{\frac{1}{2} \omega^2} \quad (\text{A.3})$$

Using the potential flow theory and equation (A.2), the added moment of inertia of a thin plate of length L and height h , rotating about an axis in the plane of the surface area of the plate, perpendicular to the direction for which L is defined is

$$I_a = 0.0078125\pi\rho L^4 h \quad (\text{A.4})$$

([Gra93] gives $I_a = 0.0078125\pi\rho L^4$, but dimensional analysis shows that a length is missing in this formula. Since the inertia of a plate not only depends on the length, but also on the height of the plate, the assumption of eq (A.4) is made. The reference for this formula in [Gra93] could not be found.)

Appendix A.3 Equivalent mass

The equivalent mass is the ‘dynamic mass’ the cylinder feels. It is defined as the mass that the cylinder feels at an acceleration of 1 m/s^2 [RexHy]

$$m_{eq} = \frac{F_{cyl}}{1 \frac{\text{m}}{\text{s}^2}} \quad (\text{A.5})$$

Here, F_{cyl} is the force needed to realise an acceleration of 1 m/s^2 .

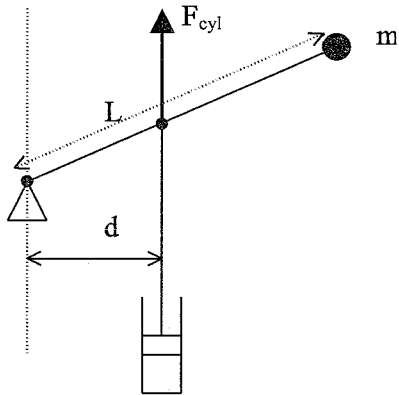


Figure A.3 rotating structure

The moment now is

$$M = I\dot{\omega} = F_{cyl} \cdot d \quad (\text{A.6})$$

$$\dot{\omega} = \frac{\ddot{x}_{cyl}}{d} \quad (\text{A.7})$$

This results in $m_{eq} = \frac{I}{d^2}$, and because $I = mL^2$,

$$m_{eq} = \frac{mL^2}{d^2} \quad (\text{A.8})$$

The situation at the lock is as figure A.4, the ratio L/d is ca. 2. This means that $m_{eq} = 4m$, with m concentrated at the centre of mass.

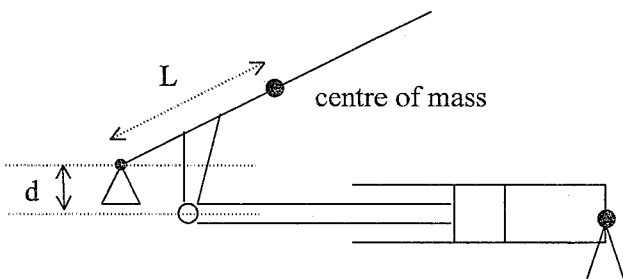


Figure A.4 Situation at lock gate

Appendix A.4 Lowest natural frequency

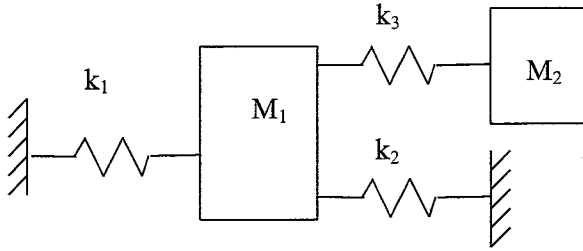


Figure A.5 Model of the cylinder and lock-gate

A model of the cylinder and lock gate and its elasticity's is figure A.5. The spring k_1 represents the stiffness of the oil column on the piston side, k_2 the stiffness of the oil column on the ring side. The spring k_3 represents the stiffness of the connection between the piston and the lock gate and the stiffness of the lock gate. Assuming the stiffness of k_3 is much higher than the oil columns, the lowest natural frequency will be

$$\omega_n = \sqrt{\frac{k_1 + k_2}{M_1 + M_2}} \quad (\text{A.9})$$

The stiffness of the oil columns is calculated by

$$k_i = \frac{A_i^2 E}{A_i L_i + V_{ineff,i}} \quad (\text{A.10})$$

where A_i is the area of the piston or the annular, E the effective bulk modulus, L_i the length of the effective oil column. The stiffness of the oil column (and so ω_n) depends on the position of the piston. The mass M_1 consists of the mass of the piston and the mass of the oil. From the drawings of the cylinder, the volume of the piston can be calculated. Also from the drawings, an estimation of the volume of oil can be made. The mass M_2 is the equivalent mass of the lock gate and the water it moves. The moment of inertia of the moving water can be calculated via Appendix A.3. Since $I = mr^2$, the added mass concentrated at the centre of mass of the lock can be calculated. The equivalent mass (appendix A.3), is (in this case) 4 times the mass of the lock gate and the added mass.

From the lowest spring stiffness, the lowest natural frequency calculated is ca. 3 Hz.

The real frequency can differ from the calculated, because some of the parameters were not known and because the springs are probably less stiff, because the oil can flow to the tank or in differential connection, to the other chamber.

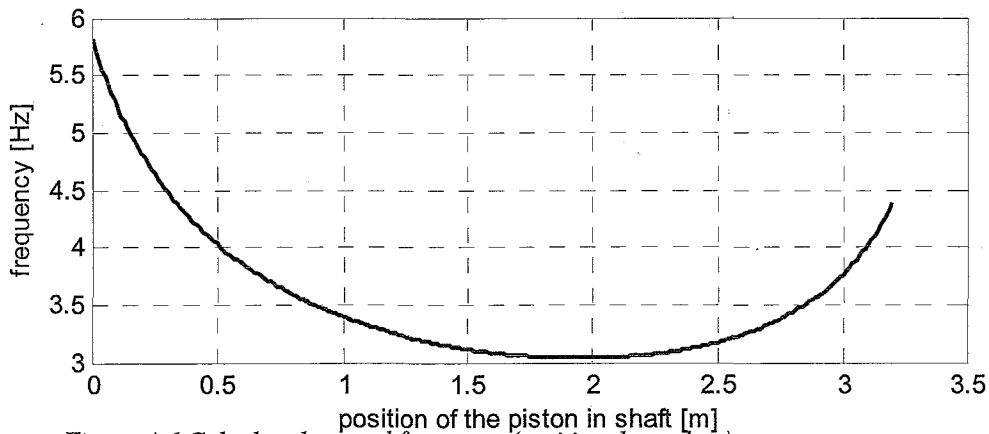


Figure A.6 Calculated natural frequency (position dependant)

Appendix B Strain Gauges

B.1 Theory of strain gauges

Strain gauges are used to measure the elongation or strain, of materials. Strain gauges consist out of a foil on which a resistance wire is installed. By gluing the strain gauge on construction part, the foil and the strain gauge should follow the deformation of the underlying material. The resistance of the resistance wire is dependent on its elongation. By measuring the change of the resistance it is in principle possible to measure the strain of the underlying construction part. In the next figure a strain gauge is shown with two measuring grids, the upper for measuring strains in vertical direction and the lower for strain in horizontal direction.

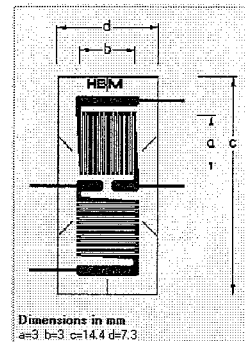


Figure B.1 Double grid strain gauge

The relationship between the strain of the strain gauge and its resistance is given by the gauge factor of the strain gauge:

$$\frac{\Delta R}{R} = k \cdot \varepsilon \quad (\text{B.1})$$

Using a normal gauge factor of 2 makes clear that the resistance changes are very small (only 0.07Ω at $100 \mu\text{m/m}$ strain with a strain gauge of 350Ω). These resistance changes can only be measured accurately with the use of a Wheatstone bridge circuit [Hof89].

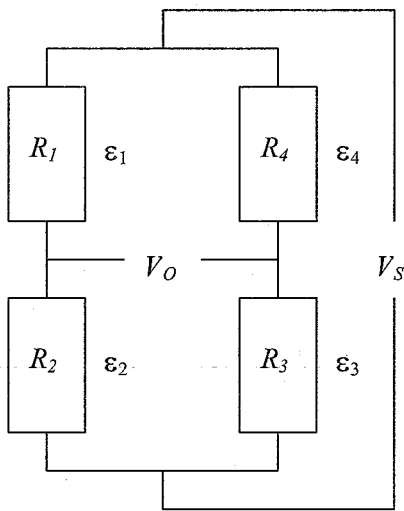


Figure B.2 Wheatstone bridge circuit

The Wheatstone bridge consists of 4 resistances (R_i) on which a certain supply voltage, V_S , is applied. The bridge gives a certain output voltage, V_O , depending on the magnitude of the resistances. The bridge is balanced (zero output) when:

$$R_1 = R_2 = R_3 = R_4 = R \quad \text{or} \quad \frac{R_1}{R_2} = \frac{R_4}{R_3} \quad (\text{B.2})$$

For a balanced Wheatstone bridge the following linearised (very small resistance changes) equation holds:

$$\frac{V_o}{V_s} = \frac{1}{4} \left(\frac{\Delta R_1}{R_1} - \frac{\Delta R_2}{R_2} + \frac{\Delta R_3}{R_3} - \frac{\Delta R_4}{R_4} \right) = \frac{1}{4} (\varepsilon_1 - \varepsilon_2 + \varepsilon_3 - \varepsilon_4) \quad (\text{B.3})$$

The last part of the equation holds as long as all 4 resistances in the bridge are active strain gauges. By applying a supply voltage (1 to 10 Volts) and measuring (after some amplification) the output voltage (order of magnitude mV) the strains can be determined. In the equation above can be seen that some resistances have a positive and some have a negative effect on the output of the bridge. By specific coupling of one or more strain gauges in the bridge circuit different mechanical quantities can be measured and en possibly some parasitic influences can be compensated. The major parasitic parameter is temperature. Temperature changes cause changes in the resistance of the strain gauges and the resistance of the connecting wires. A temperature change also causes a deformation of the underlying material by thermal expansion of the material. The final objective of the strain measurements is the determination of stresses for the calculation of the external loads. Strain as a result of thermal expansion must therefore not be present in the calculation of the loads.

In [Hof89] some methods of temperature compensation are presented. For example when using a quarter bridge (one active strain gauge) temperature compensation is possible by using a compensation strain gauge on a unloaded piece of material with the same temperature as the test object, connected to the second arm of the bridge.

In this case the objective of the strain gauge measurements is the measuring of axial force in the piston rod. Measuring with one strain gauge using a quarter bridge suffers from two parasitic influences; the above mentioned temperature effect and the bending strains in the piston rod. In [Hof89] a configuration is presented using 4 active strain gauges which, in theory, compensate for both temperature as bending effects. In a beam loaded in axial and transverse direction a one-dimensional stress state exists with normal stresses in axial direction. These stresses consist of the axial stresses caused by the axial load and bending stresses caused by the bending moments introduced by the transverse load:

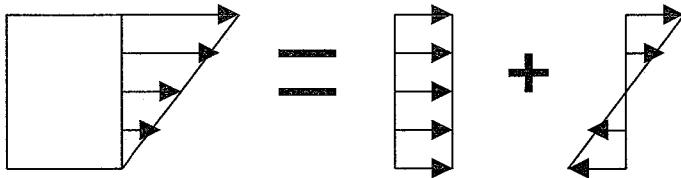


Figure B.3 Superposition of axial and bending stresses.

In a one-dimensional stress state the following relationship between normal stress, σ_n , and normal strain, ε_n , (Hooks law) holds:

$$\sigma_n = E \cdot \varepsilon_n \quad (\text{B.4})$$

Here is E the Young's modulus of elasticity, a material parameter. When 4 strain gauges are glued onto a bending beam; two in axial direction at exactly 180° opposite to each other and two on exactly the same location but in transverse direction, the bridge gives an output independent on temperature and bending in the beam. The following relations hold for the 4 strains of the strain gauges:

$$\varepsilon_1 = \varepsilon_l + \varepsilon_b + \varepsilon_{\theta,1} \quad (\text{B.5})$$

$$\varepsilon_2 = -\nu \cdot (\varepsilon_l + \varepsilon_b) + \varepsilon_{\theta,2} \quad (\text{B.6})$$

$$\varepsilon_3 = \varepsilon_l - \varepsilon_b + \varepsilon_{\theta,3} \quad (\text{B.7})$$

$$\varepsilon_4 = -\nu \cdot (\varepsilon_l - \varepsilon_b) + \varepsilon_{\theta,4} \quad (\text{B.8})$$

Here ε_l is the longitudinal strain caused by the axial load, ε_b the bending strain, $\varepsilon_{\theta,i}$ the indicated strain caused by thermal effects (thermal expansion and thermal resistance changes) on the strain gauge specific location and ν the Poisson ratio of the material. When it is provided that the thermal strains for all the strain gauges in the bridge circuit are the same, the following hold for the output of the bridge:

$$\frac{V_o}{V_s} = \frac{k}{4} (\varepsilon_1 - \varepsilon_2 + \varepsilon_3 - \varepsilon_4) = \frac{k}{4} 2(1 + \nu) \varepsilon_l = \frac{k}{4} \varepsilon_l \quad (\text{B.9})$$

Because the bridge adds all the axial strains the bending strains compensated because they are positive on one side and negative on the other. The thought that only bending strains in the plane of the strain gauges are compensated is not true. Every combination of bending moments in a bending beam can be represented by two perpendicular bending moments with arbitrary direction. When the maximum values of one bending moment are aligned with the location of the strain gauges the second bending moment has its neutral axis aligned with the strain gauges, resulting in no bending strain at the location of the strain gauges caused by the second bending moment. The bridge adds two thermal strains and subtracts two thermal strains resulting in no thermal output of the bridge. What remains is an output of the bridge that is only dependent on the axial force on the beam. For the axial force on the cylinder holds:

$$F = \sigma_l \cdot A = E \cdot \varepsilon_l \cdot A = \frac{\varepsilon_l \cdot E}{2(1 + \nu)} \cdot A \quad (\text{B.10})$$

B.2 Sources of errors

Error made with respect to the theoretical ideal compensation for temperature and bending are caused by:

1. Unequal temperature sensitivity of different parts of the bridge circuit.
 2. Temperature gradients within the bridge circuit.
 3. Unequal sensitivity (gauge factor) of the strain gauges
 4. Geometrical errors due to imprecise gluing of the strain gauges.
 5. Other stresses in the beam then calculated using the analytical formulas for axial stress and bending.
1. Unequal temperature sensitivity of the different parts of the bridge will result in a thermal output of the bridge. Strain gauges are available with different thermal constants. Choosing a thermal constant close to the thermal constant of the material it is glued on significantly reduces the thermal output. The residual effects can be minimized by making the bridge as symmetrical as possible. This means using of equal strain gauges (preferably from the same production batch), using equal lengths of the wires for the arm within the bridge.
 2. When temperature gradients exists within the bridge, the strain gauges with their wires are exposed to different temperatures. Even with equal temperature sensitivity of the strain gauges and the wires, a thermal output will result. Temperature gradients on the piston rod are expected to be present in horizontal as well as in vertical direction. But because the location of the axial and transverse strain gauge on one side are the same, still optimal thermal compensation is achieved because the axial and transverse direction are subtracted from each other. Even when a different temperature between the two sides of the rod is present, every side takes care of its own temperature compensation.
 3. A difference in gauge factor is always present which can be minimized using strain gauges from the same batch. Usually a tolerance band of $\pm 1\%$ is specified. This results in a small thermal output of the bridge and some superimposed bending strain on the measuring signal. How large

these effects are depends on the magnitude of the temperature changes during the measurements and the ratio between the axial strains caused by the axial load and the bending strain.

4. Two geometrical mistakes can be made; improper alignment of the strain gauge with the axial direction of the rod and unsymmetrical alignment of the strain gauges on one side with respect to the other side. The result of the first mistake results in a 1-cosine error in determining the axial strains. The second mistake results in two errors. For compensating the bending strains of the bending moment in the plane of the strain gauges a 1-cosine error is made due to reduction of the distance to the neutral axis in case of a round beam, piston rod in this case. For the bending moment in the other direction however, an alignment error introduces an offset with respect to the neutral axis of this particular bending moment. This is a linear error (sine for very large misalignments on a round beam).
5. When calculating stresses and loads out of the measured strain analytical formulas are used. The errors made using these formulas lies in the inexact parameters in the formula; inexact values of the material parameters E and ν , the geometrical tolerance of the rod A (negligible) and in the inexact representation of reality by the formula itself. The calculation of the axial load is based on the assumption of a homogeneous axial stress, and the bending formula

Errors due the un-ideal thermal compensation can thus be minimized by making the bridge as symmetrical as possible and maintaining the temperature as constant as possible. Location of the strain gauges on the rod (top/down or left/right) does not influence this. For locating the strain gauges mechanical compensations are important. First a considerable distance from the end of the rod is necessary for providing a homogeneous stress state, 2 to 3 times the rod diameter will be enough. Second, the angular placement of the stain gauges must be chosen. Two basic choices exist; top/down or left/right. Here is chosen for a left/right placement of the strain gauges on the rod, this because of the accessibility at this location. Then the bending moment in the horizontal plane (introduced by the friction moment in the end bearings of the cylinder) are compensated. Misalignment of the strain gauges only introduces a 1-cosine part of the friction moments in the measurement, the bending moment in the vertical plane (introduced by weight of the cylinder) however, is introduced linear in the measurement signal.

B.3 Level of bending moments in the piston rod

B.3.1 Bending in vertical plane

The bending moments in the vertical plane are introduced by the weigh of the cylinder. For calculating the bending stresses in the rod three models, rising in sophistication are used:

1. Single beam with constant distributed load over entire length of the cylinder
2. Two beams with each their own distributed load connected at two points with each other
3. Modelling cylinder in the DBR (Deflection and Buckling Routine). This is a finite element program for calculation the deflection of a hydraulic cylinder. Various loads, masses of different parts and bearing clearances, resulting in non-colinearity of centerlines of shell and rod, can be modelled.

Single beam:

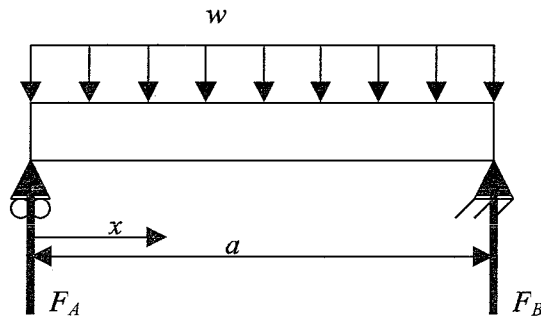


Figure B.4 Single beam model

For the bending moment as a function of the position (x) holds [Fen93]:

$$M_b(x) = \frac{w}{2}(ax - x^2) \quad (\text{B.11})$$

Double beam:

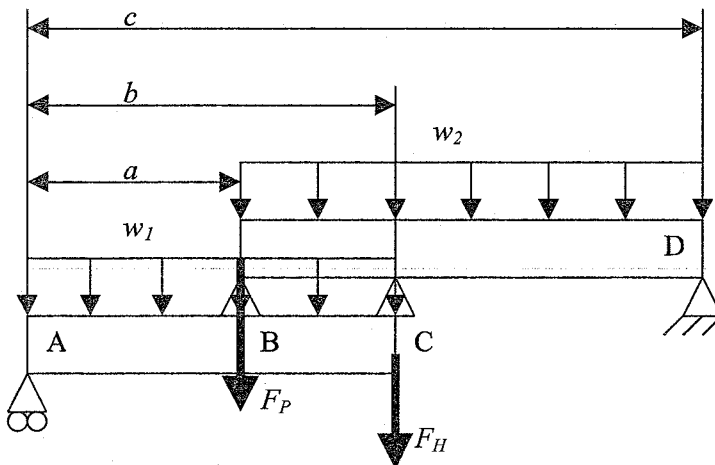


Figure B.5 Double beam model

Again, from [Fen93] can be derived:

Moment around A:

$$M_A = \frac{w_1 b^2}{2} + \frac{w_2 (c-a)(c+a)}{2} - F_P a + F_H b + F_D c \quad (\text{B.12})$$

Then F_D is:

$$F_D = \frac{w_1 + w_2 (c^2 - a^2) + 2(F_P a + F_H b)}{2c} \quad (\text{B.13})$$

Out of force equality in vertical direction follows for F_A :

$$F_A = w_1 b + w_2 (c - a) - F_P + F_H + F_D \quad (\text{B.14})$$

With these boundary conditions the following free body diagram can be constructed:

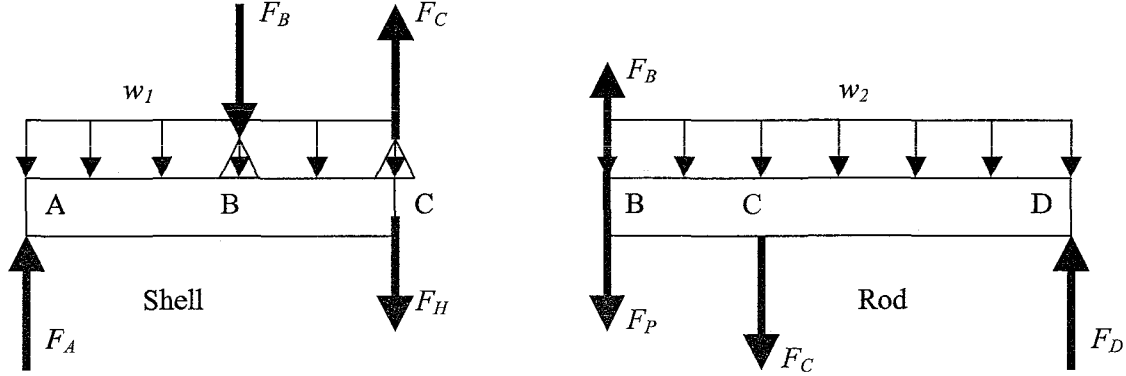


Figure B.6 Decoupled double beam model

Moment equality around C for the Shell:

$$M_{C,S} = F_A b - F_B (b - a) - \frac{w_1}{2} = 0 \quad \Rightarrow \quad F_B = \frac{F_A b - \frac{w_1 b^2}{2}}{(b - a)} \quad (\text{B.15})$$

Moment equality around A for the Shell:

$$M_A = \frac{w_1 b^2}{2} + F_B a - F_C b + F_H b \quad \Rightarrow \quad F_C = \frac{\frac{w_1 b^2}{2} + F_B a + F_H b}{b} \quad (\text{B.16})$$

For the shear forces and bending moments in the shell part holds (x starting at left end of shell):

$$V_S(x) = \frac{dM_S}{dx} = F_A - w_1 x, \quad M_S(x) = F_A x - \frac{1}{2} w_1 x^2 \quad \text{for } x = \langle 0, a \rangle \quad (\text{B.17})$$

$$V_S(x) = \frac{dM_S}{dx} = F_A - F_B - w_1 x, \quad M_S(x) = (F_A - F_B)x - \frac{1}{2} w_1 x^2 + C_S \quad \text{for } x = \langle a, b \rangle \quad (\text{B.18})$$

$$M_S(b) = 0 \quad \Rightarrow \quad C_S = \left[\frac{1}{2} w_1 x^2 - (F_A - F_B)x \right]_{x=b} = \frac{1}{2} w_1 b^2 - (F_A - F_B)b \quad (\text{B.19})$$

For the shear forces and bending moments in the rod part holds (x starting at left end of rod):

$$V_R(x) = \frac{dM_R}{dx} = (F_B - F_P) - w_2 x, \quad M_R(x) = (F_B - F_P)x - \frac{1}{2} w_2 x^2 \quad \text{for } x = \langle a, b \rangle \quad (\text{B.20})$$

$$V_R(x) = \frac{dM_R}{dx} = F_B - F_P - F_H - w_2 x,$$

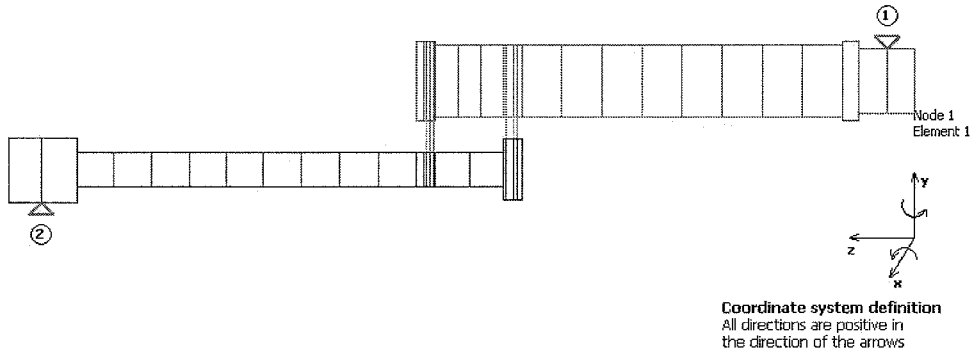
$$M_R(x) = (F_B - F_P - F_H)x - \frac{1}{2}w_2x^2 + C_R \quad \text{for } x = \langle b, c \rangle \quad (\text{B.21})$$

$$M_S((c-a)) = 0 \quad \Rightarrow$$

$$C_R = \left[\frac{1}{2}w_2x^2 - (F_B - F_P - F_H)x \right]_{x=(c-a)} = \frac{1}{2}w_1(c-a)^2 - (F_B - F_P - F_H)(c-a) \quad (\text{B.22})$$

DBR-model

The Deflection and Buckling Routine (DBR) is a finite element program for calculating the deflection and buckling behaviour of a hydraulic cylinder, developed by Rexroth Hydrauldyne in co-operation with the Eindhoven University of Technology. In this routine the shell and rod group are both modelled by a series of beam elements. The two parts are connected with Non-linear spring elements, representing the bearing strips in the cylinder. The final model is solved using a non-linear solving procedure. In the next figure a finite element model produced by the DBR is shown:



Number of generated elements : 51
 Number of generated nodes : 47

Support Reactions

	F(z) [N],	F(x) [N],	F(y) [N],	M(x) [Nmm],	M(y) [Nmm]
Support: 1	100000	0	22377	0	0
Support: 2	0	0	18174	0	0

Figure B.7 Finite element model produced by the DBR.

Results

In the next three figures the calculated bending moments for the three different calculating methods are shown.

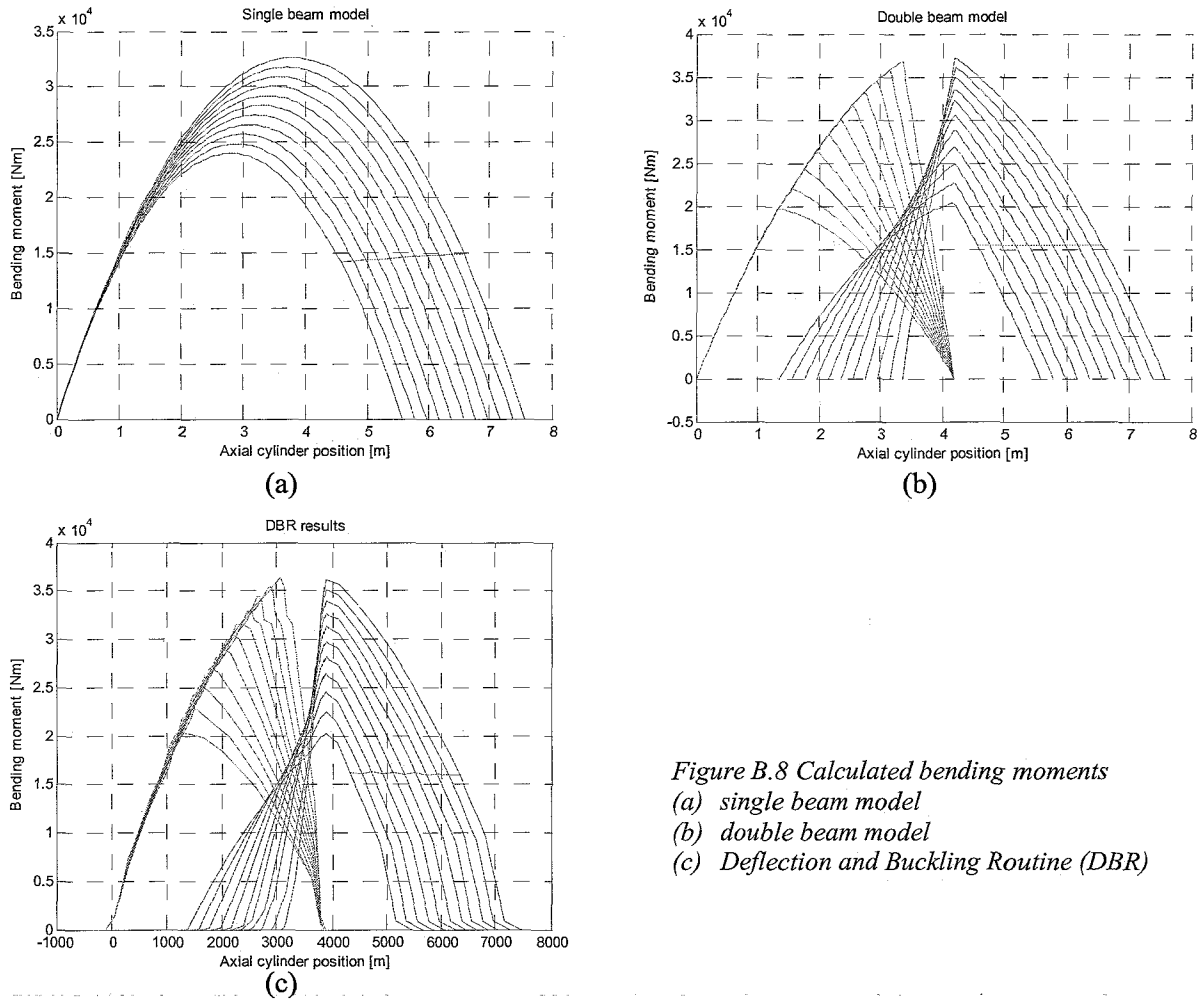


Figure B.8 Calculated bending moments
 (a) single beam model
 (b) double beam model
 (c) Deflection and Buckling Routine (DBR)

Comparing the methods

The first method, using a single beam model, gives only a rough indication of the order of magnitude of the occurring bending moment (which in this case is enough). The other two methods give more accurate results. The double beam model gives results that are very similar to that of the DBR. Therefore it can be concluded that this method is accurate enough for calculating bending stresses in the cylinder parts. The bending stress at the location of the strain gauges is indicated in figure B.8 a-c. Although the bending moments are relatively high, they don't change much. A non-optimal bending stress compensation gives only a zero point shift of the bridge, which stays relatively constant during the measurements. In the next table the change of the bending moment, stresses and strains during the measurements are shown.

	Bending Moment [Nm]		Bending stress [N/mm ²]		Bending strain [μm/m]	
	Retracted	Extended	Retracted	Extended	Retracted	Extended
Single beam	1.413*10 ⁴	1.494*10 ⁴	13.52	14.29	64.98	68.71
Double beam	1.552*10 ⁴	1.540*10 ⁴	14.85	14.73	71.38	70.83
DBR	1.630*10 ⁴	1.595*10 ⁴	15.59	15.26	74.96	73.35

Table B.1 Bending moments

B.3.2 Bending moments in horizontal plane

The bending moments in the horizontal plane are introduced by the friction moments in the spherical end-bearings of the cylinder. The direction of these friction moments is opposite to the direction of rotation of the particular end-bearing. Stress analyses of these loads can be done analytical. The bending moment in the horizontal plane is the super position of the two bending moments introduced by the spherical end-bearings. One applied moment at the end of a simply supported beam results in a linear decreasing bending moment across the beam.

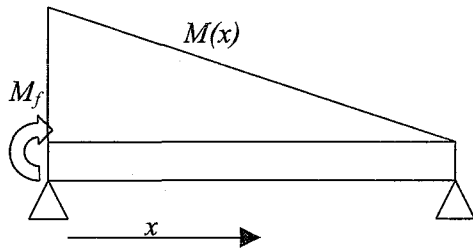


Figure B.9 Bending moment in beam

The superposition of the two bending moments results in a linear varying bending moment across the beam. The end values are simply the friction moments at the end of the beam. The friction moment can be estimated with the next formula:

$$M_f = F_f \cdot r = F_{ax} \cdot \mu \cdot r \quad (B.23)$$

With an axial force, F_{ax} , of 100 kN, a friction coefficient μ of 0.1 and a friction radius r of 0.125 m, a friction moment of 1250 Nm results. This is one order of magnitude smaller than that in the vertical plane, but it varies constantly during the measurements. Every time the direction of rotation in the spherical bearing changes the friction moment changes. This occurs at a change of direction of the cylinder for both bearings, but also somewhere in the mid-stroke of the cylinder for the bearing at bottom side. In the figure (B.10) can be seen that the cylinder turns to and from the lock wall during its stroke:

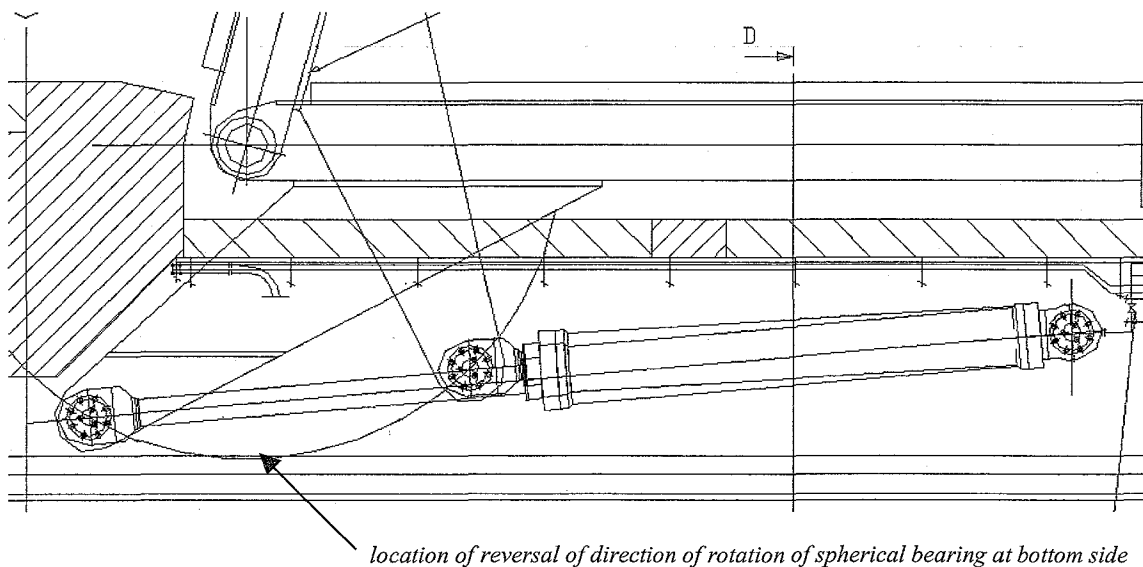


Figure B.10 Geometry and movement of the cylinder.

This effect has been measured. During the first test the connecting leads of the strain gauges bridge were not properly connected. Instead of compensating the bending strain, the axial was compensated and only bending in horizontal plane was measured. The same behaviour can be calculated based on geometrical analysis of the construction as can be seen in the figure (B.11).

The 'jump' is not on exactly the same position, but this may be caused by the non accurate sketch on which the geometrical relations have been measured. The location of the change of direction of rotation was determined experimentally using a dial indicator (fig B.12)

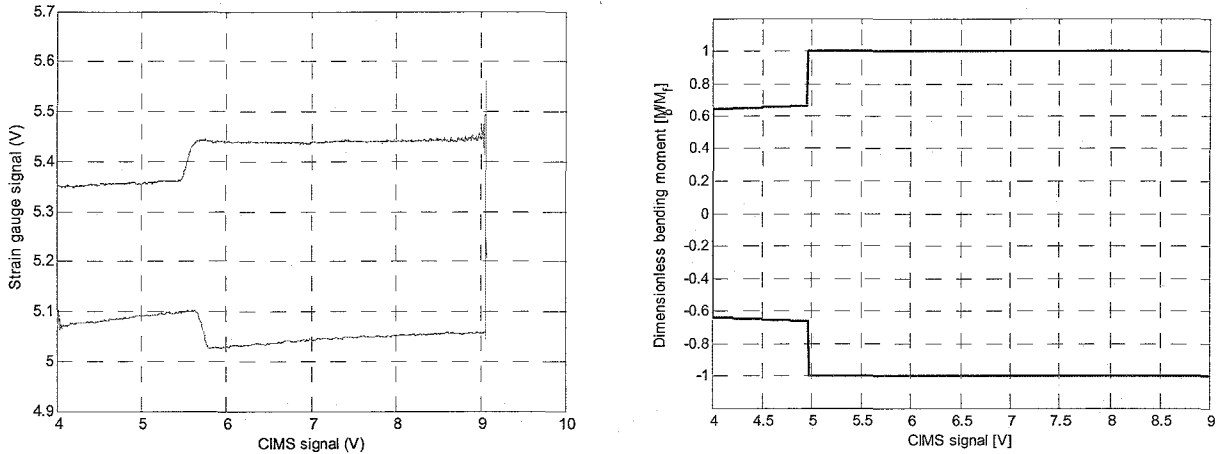


Figure B.11 Change of direction of friction moment a) measurement b) calculation

Experiments showed the a change of rotation from CIMS signal 5.5 to 5.65 V for ingoing and 5.65 to 5.8 V for outgoing motion, just as in the strain gauge measurements. The 'jump' in the bending measurements equal 0.325 times one friction moment as can be seen in the right diagram. The 'jump' in the measurement equals 0.07-0.08 Volts. The bending stress can be calculated by equation (B.24). Here, V_{out} is the output signal of the strain gauge amplifier and Sen is the sensitivity setting of the strain gauge amplifier.

$$\sigma_b = \frac{4 \cdot V_{out} \cdot Sen \cdot E}{10 \cdot 2(1 + \nu)k} \quad (B.24)$$

This results in a bending stress of 0.26-0.30 N/mm². This equals a bending moment of 272-314 Nm. This being 0.325 of the friction moments gives an approximation of the friction moments of the spherical bearings of 836-965 Nm. The order of magnitude is the same as the above estimated friction moment (equation B.23), but the axial force in the cylinder was not 100 kN as shown later but around 10 kN. The relative high bearing load for the low axial load on the cylinder is caused by the fact that the spherical bearings are loaded in their axial direction by the weight of the cylinder. The load in axial direction of the bearing is also around 20 kN. This results in a loading direction for which the spherical bearing was not intended. A wedging effect in the spherical bearing may cause the relative high friction moment in the bearing.

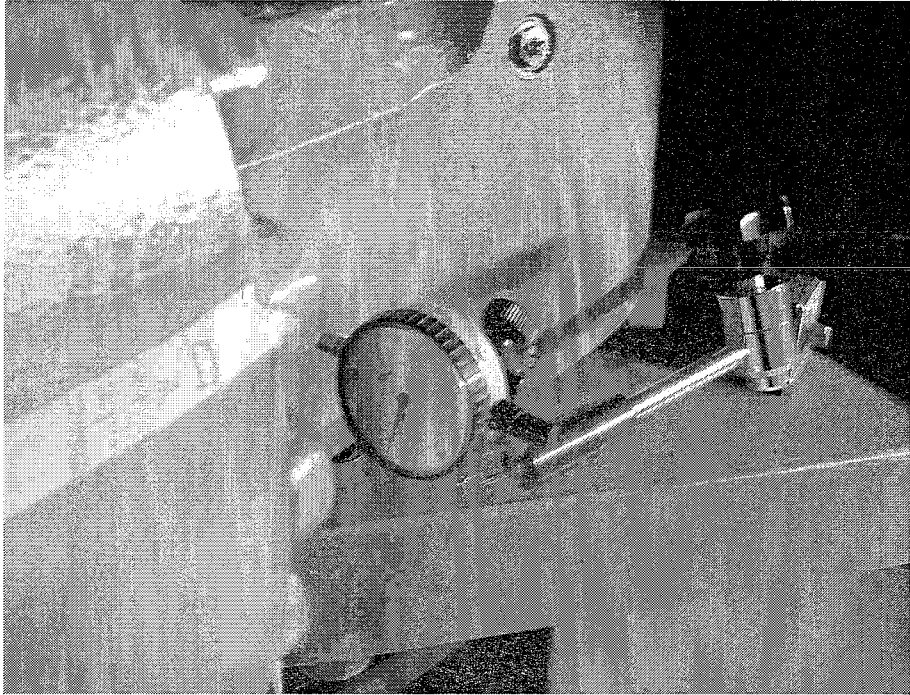


Figure B.12 Photo dial indicator for locating the change of direction of

Appendix C: Experiments with test rods

Experiments were done with test rods (fig C.1) on a tensile strength tester at the department of architecture, building and planning of the Eindhoven University of Technology.

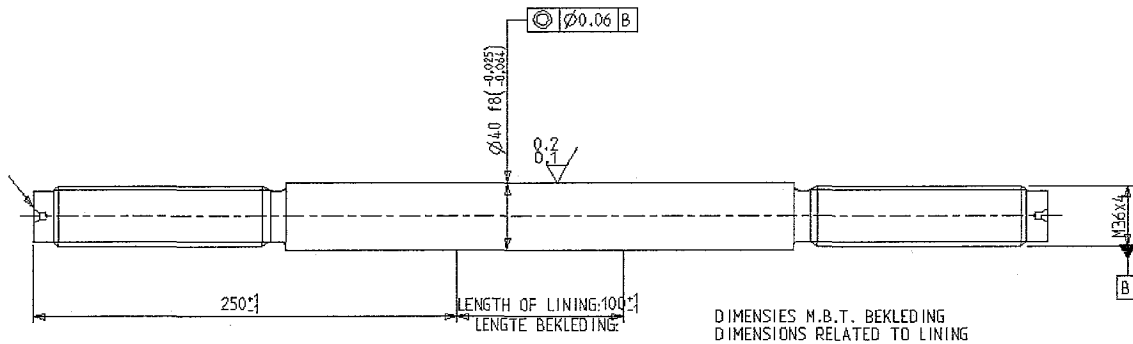


Figure C.1 Design of test rods

C.1 Purpose of the test measurements

The purpose of taking measurements on test rods in a tensile strength tester is

1. to determine the distribution of the strain gauge factor,
2. to determine the elastic modulus,
3. to investigate whether the CERAMAX-layer has influence on the measurement,
4. to investigate the effect of bad alignment and air bubbles under the strain gauge.

(1) The distribution of the strain gauge factor (k)

The K-factor gives the relationship between the voltage ratio V_{out}/V_{in} of the Wheatstone-bridge and the strain of one strain gauge.

The manufacturer provides the strain gauge factor. For the strain gauges used, it is $1.98 \pm 1\%$. This gives a 1 % uncertainty on the measured force.

(2) The elastic modulus

The elastic modulus for steel (all mentioned variants) is $200 \cdot 10^9$, according to [Poly03]. According to [Fen93], the elastic modulus for steel is $207 \cdot 10^9$. Hydraudyne uses an elastic modulus of $211 \cdot 10^9$. This would give: $E = 205.5 \cdot 10^9 \pm 2.7\%$, which is much larger than the uncertainty of the strain gauge factor ($\pm 1\%$). The question to be answered is: what is the elastic modulus of the material, and: does it change with a different type of steel? For this purpose, 2 different types of steel are tested: St52 and 42Cr. The steel used in the lock is St52.

(3) Influence of CERAMAX-layer

The CERAMAX-layer on the rods is a porous ceramic elastic layer of thickness 300 μm . It is not known whether it exhibits internal shearing. In the measurements on the lock, the strain gauges will be glued to the rod at at least 3 times the diameter. In the test measurements the strain gauges are glued to the middle of the rod, which is 15 cm ($3.5 \cdot D$) from the ends. If the calculated elastic modulus is lower than expected ($< 200\text{-}211 \cdot 10^9$), the CERAMAX-layer probably has an effect on the measurements.

(4) Influence of bad bonding and bad alignment

If the bonding of the strain gauge on the rod is bad, the strain in the strain gauge is lower than the strain in the rod, and faulty measurements will be done. Causes of bad bonding are air bubbles under the strain gauge (especially under the grid) and bad bonding of the glue caused by an unclean surface. Air bubbles are easily seen due to colour differences. Since the strain in the axial direction is largest, bad alignment will result in lower strain measurement.

At an angle error φ , the measured stress and strain will be:

$$\varepsilon_m = \frac{1}{2} \varepsilon_a [1 - \nu + \cos(2\varphi)] * (1 + \nu) \quad (C.1)$$

$$\sigma_m = \frac{1}{2} \sigma_{\max} (1 + \cos(2\varphi)) \quad (C.2)$$

The strain gauge has a length of 15 mm. Table C.1 gives the error for alignment errors of 0.5 and 1 mm.

In table C.2 the alignment error on the test rod are specified.

alignment	φ	$\varepsilon_a/\varepsilon_m$	σ_{\max}/σ_m
1mm/15mm	3,8	1.00579	1.00444
0.5mm/15mm	1,9	1.00144	1.00111

Table C.1 Effects of bad alignment

C.2 Experiments

The experiments are done on a 250 kN tensile strength tester. The force is measured in the tester and the output of the strain gauges bridge is measured with a MGC⁺ amplifier from HBM. The amplifier provides a carrier frequency of 4.8 kHz for the input voltage of the bridge to suppress disturbances. A comparative test is done with the amplifier to be used in the measurements on the lock (SGA amplifier from Mantracourt).

Calibration

$$F = EA\varepsilon = EA * \frac{1}{2(1+\nu)} * \frac{4}{k} * \frac{V_{uit}}{V_{in}} \quad (C.3)$$

Tensile strength tester

The tensile strength tester was calibrated 2 months earlier and gives an output of 10 V at 250 kN. Before the measurement, the zero point of the force is put on the zero point of the voltage.

$$1V = 25 \text{ kN}$$

The amplifiers were calibrated with a loadcell simulator, using shunted bridge circuits.

MGC⁺ amplifier

$$-1000 \mu\text{m/m} = 0.5 \text{ mV/V at } k = 2 \rightarrow 4.024 \text{ V}$$

$$1V = 251.02 \mu\text{m/m at } k=1.98$$

SGA-amplifier

$$-1000 \mu\text{m/m} = 0.5 \text{ mV/V at } k = 2 \rightarrow 4.1667 \text{ V}$$

$$1V = 242.42 \mu\text{m/m at } k=1.98$$

Shunt calibration provides the same calibration factor as calibration with the loadcell simulator.

Experiments

The velocity of the tensile strength tester was 6 mm/min. Each rod of Cr42 runs through 3-5 cycles of -125 kN to 250 kN. The rods of Steel52 run through cycles of -125 to 125 kN. The measurements were done with a sample frequency of 128 Hz. With a least squares fit the slope of the (tensile force voltage, strain gauge bridge voltage) is calculated. The results can be found in table C.2

rod	material	amplifier	bonding	alignment [mm/15mm]	slope	E at k = 1.98 and v = 0.3 *10 ⁹	deviation with respect to rod 1 in %	mean std *10 ⁹
1	42Cr	MGC ⁺ SGA	questionable	0.5/0.5	0,9983 0,9617	205.71 205.20	-- -0,25	mean 205.57
2	42Cr	MGC ⁺	poor	<0.5/0	0,9956	205.15	-0,27	std 0.444
3	42Cr	MGC ⁺	well	1/<0.5	0,9959	205.22	-0,24	
4	42Cr	MGC ⁺	well	<0.5/0	1,0006	206.18	0,23	
5	42Cr	MGC ⁺	well	1/0.5	0,9995	205.96	0,12	
6	St52	MGC ⁺	well	<0.5/0	1,0078	207.67	0,95	mean 208.52
7	St52	MGC ⁺	poor	1/0	1,0075	207.61	0,92	
8	St52	MGC ⁺ MGC ⁺	well well	<0.5/0	1,0159 1,0166	209.34 209.48	1,76 1,83	std 1.02

Table C.2 Results of test measurements

Remarks

- The noise level on the measurements with the SGA is comparable with the noise level on the MGC⁺. The noise for both is just 2 or 3 bits.
- The measurement goes through a hysteresis loop, but this can be partly explained by the time delay introduced by the low pass filter (10 Hz) on the force measurement. The time delay is ca. 0.02 s. With the original low pass filter (2 Hz), this was 0.15 s.
- The tensile strength test exhibits a zero point shift, which can not be separated from the zero point shift of the strain gauge bridge.

C.3 Conclusions

- There is a clear difference between the elastic moduli for steel52 and chrom42. For the experiments on the lock (St52), an elastic modulus of $208 \cdot 10^9$ will be used.
- No effect of the CERAMAX layer is seen in the measurements. The results are as expected.
- The measurements of one particular material have a maximum difference of 0.9 %, this is well within the $\pm 1\%$ uncertainty of the gauge factor.
- The effect of bad alignment and bad bonding can not be clearly seen in the measurements, since the differences stay within the $\pm 1\%$ uncertainty of the gauge factor. It in this case the effect can not be large, since the rods 2 and 7, which were expected to perform poor, due to air bubbles, are performing the same as other rods.

Appendix D Measurement equipment

D.1 Pressure transmitters

Two different pressure transmitters were used. One Keller pa 21 and four Hydac HAD 4744-A-400-000. Both are piezoresistive pressure transmitters.

	Hydac	Keller
Signal output	4-20 mA	4-20 mA
Measurement range	0 - 400 V	0 - 400 V
Total error band (0 ..+50°C)		1.0 % FS max
Temperature compensation		
zero-point	$\leq \pm 0.08$ FS/10K typ $\leq \pm 0.15$ FS/10K max	$\leq \pm 0.1$ FS/10K typ $\leq \pm 0.2$ FS/10K max
sensitivity		$\leq \pm 0.1$ /10K typ $\leq \pm 0.2$ /10K max
Hysteresis	$\leq \pm 0.4$ % FS max	
Repeatability	$\leq \pm 0.1$ % FS max	
Linearity	$\leq \pm 0.4$ % FS max	

Table D.1 Some specification of the pressure transmitters [Keller], [Hydac]

For calibration, the pressure transducers were connected to a 0.2 class manometer calibration device and measurements for 0 to 25 bar were taken. This provided the used gain of the pressure transducers. The used zero-point comes from zero point measurements in the field.

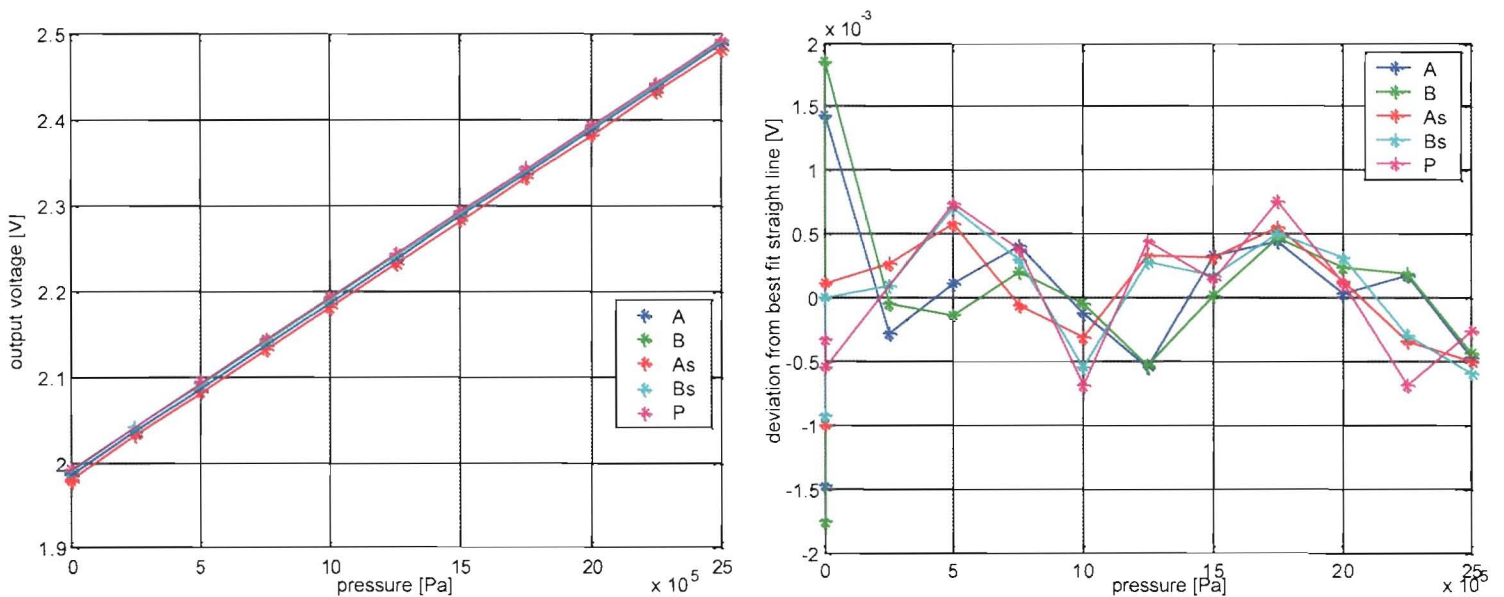


Figure D.1 Calibration of the pressure transducers

Pressure transducers used on:

A: base side of cylinder [hydac]. B: annular side of cylinder [hydac], As: Base side of hydraulic system [hydac],

Bs: annular side of hydraulic system [hydac], P: close after pump [keller]

(a) determining gain and zero point

(b) determining linearity

D.2 Accelerometer

Type	MNT/7220Q-5
range	+/- 5 g
output signal	4-20 mA
sensitivity	1.595 mA/g
offset bias	11.935 mA

Table D.2 Some specifications of the accelerometer

Calibration measurements are done by way of measuring the output at +g, -g and 0 g. To take these measurements, a flat measurement table was used. The output at 0 g is measured with the accelerometer at angles 0,90,180 and 270 degrees from the original position (in a measurement V).

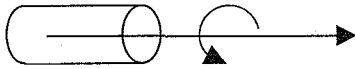


Figure D.2 position of accelerometer

The results are:

	output voltage {V}
g	6.7520
-g	5.1526
0	5.9411
90	5.9693
180	5.9567
270	5.9311

Table D.3: calibration results of accelerometer

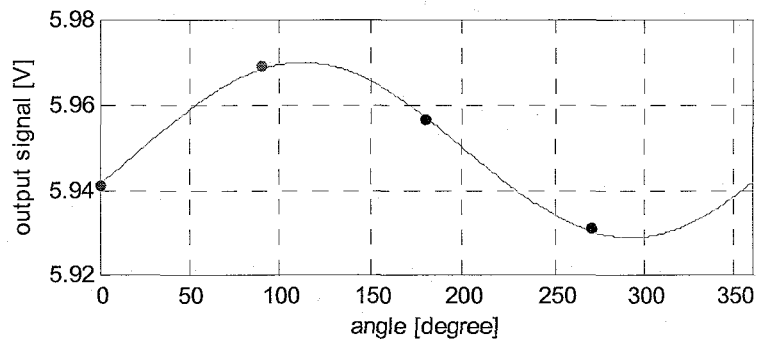


Figure D.3 determining angle error of accelerometer

This comes to a sensitivity of 0.8 V/g (1.6 mA/g) and an offset bias of 5.952 V (11.905 mA). From these measurements, it can also be concluded that the measurement device inside the accelerometer is mounted under an angle. An angle error of 1.5° was determined by fitting a sine function through the measurements of 0 g (see fig (D.3)).

D.3 Strain gauges and amplifier

D.3.1 strain gauges

The used strain gauges were HBM strain gauges type 1-XY11 – 3/350). This are strain gauges with each 2 perpendicular measuring grids. They have a carrier and cover of polyimide and a measuring grid foil of Constantan. The measuring grid length is 3 mm and the measuring grid resistance is 350 Ohms. They are temperature-adjusted for ferritic steel ($\alpha=10.8 \cdot 10^{-6} /K$). The used adhesive is Z70.

Gauge factor	1.98±1%
operation temperature range	-70.....+200
mechanical hysteresis	
1st load cycle	1 µm/m
3rd load cycle	0.5 µm/m

Table D.4 Some specifications of the strain gauges [HBM]

D.3.2 Strain gauge amplifier

The used strain gauge amplifier is SGA strain gauge transducer amplifier from Mantracourt. It offers sensitivity settings down to 0.06 mV/V and should provide calibration possibilities (zero point and sensitivity) for each sensitivity setting. In this case the calibration for the lowest two sensitivities (0.06 mV/V and 0.11 mV/V) was not possible, so the 0.23 mV/V setting was used.

Linearity	0.03% FS
Bandwith (no filter & > 2 mV/V)	DC – 6 kHz
filter cut-off (switchable ranges)	1 – 5000 Hz (10Hz was used)
Gain stability (1st 1000 hours)	0.2 % FS
zero temperature coefficient (@2.5 mV/V)	typ 0.002 %/°C
Span temperature coefficient	typ 0.007 %/°C

Table D.5 Some specifications of the strain gauge amplifier [Mantra]

D.4 Laser vibrometer

A laser vibrometer from Polytec is used to measure the displacement and velocity of the rod. The laser head sends out a HeNe light beam and receives the reflected beam from a target. The two beams, the output and reflected beam have different phase, since different distances are travelled. If the target is moving, the phase difference will be time dependent with frequency F_D (Doppler effect, $F_D=2v/\lambda$). The phase shift is measured.

For the measurement of the displacement the displacement decoder counts the times the output signal has undergone a phase shift of 2π rad. The amount of complete signal periods is a measure of the total displacement of the object (with resolution of $\lambda/2$, which is 316.4 nm). Since the phase changes continuously with the object displacement, displacements smaller than $\lambda/2$ can also be measured.

Measurement range	Full scale output	Resolution	Max signal bandwidth	max
Velocity				
mm/s/V	mm/s	$\mu\text{m/s}$	kHz	Acceleration (g)
5	100	0.5	250	8,000
25	500	2	250	25,000
125	2,500	5	250	200,000
Displacement				
$\mu\text{m/V}$	mm	μm	kHz	Velocity (m/s)
0.5	0.008	0.002	25	0.06
2	0.032	0.008	75	0.25
8	0.13	0.032	75	1
20	0.32	0.08	250	1.6
80	1.3	0.32	250	1.6

Table D.5: measurement ranges for the vibrometer

	Velocity	Displacement
calibration accuracy	$\pm 2.5\%$ of rms reading in full operating temperature range	$\pm 2\%$ of reading ± 1 step (up to 100 kHz)
Linearity error	max $\pm 1\%$ for one particular range	± 2 steps
output swing	± 10 V	± 8 V

Table D.6 Some specifications of the vibrometer

D.5 SigLab

D.5.1 specifications

Number of channels	4 (up to 4 SigLab devices can be coupled)
type	Differential with 500 Ω low side to ground
noise floor	< -128 dB V_{rms}/\sqrt{Hz} from 1.25 to 500 Hz
voltage ranges	10 ranges: ± 20 mV to ± 10 V full scal in 6 dB steps
coupling	DC/AC(AC -3 dB point = 0.25 ± 0.05 Hz)
offset drift	$\pm 200 \mu V/^{\circ}C$ on 5 and 10 V input ranges $\pm 50 \mu V/^{\circ}C$ on all other ranges (after calibration)
residual DC offset	DC coupled: ± 1 mV $\pm 0.02\%$ of ranges + offset drift AC coupled: ± 2 mV $\pm 0.03\%$ of ranges + offset drift
absolute accuracy	$\pm 0.0025\%$ of selected full scale range
Data converter	Sigma-delta A/D, 16 bit resolution
Alias protection	90 dB on all frequency ranges for $f < 250$ kHz

Table D.7 Some specifications of SigLab

D.5.2 Offset drift

Like all data acquisition systems, SigLab experiences thermal drift. In tabel D.7, this drift is specified. To avoid large drifts, a warming up period of the data acquisition system is used. There is no specification of the required warming up time.

To gain more knowledge about warming up time and total drift, an experiment is done. A SigLab device is connected to the computer, but no input signals are given. If now SigLab measures its channels, a dc offset can be measured. This offset will also be present when a signal is connected to the channel. The experiment is done with 2 different SigLabs and 2 different input ranges (± 5 V and ± 20 mV). The results are shown in figure (D.4)

In figure D.4a, the drift is seen for a voltage range of ± 5 V. The largest drift is ca. 24 mV. Stabilisation takes up to 1.5 hours. For the ± 20 mV range (figure D.4b) the drift is much smaller in absolute sense, but much larger relatively seen. Stabilisation takes as much time as the drifts in the ± 5 V range.

Conclusion

The offset drift of SigLab is not for all channels within specifications. The warming up time can be up to 1.5 hours. If these small errors influence the quality of the measurement, a suitable long warming up time is necessary.

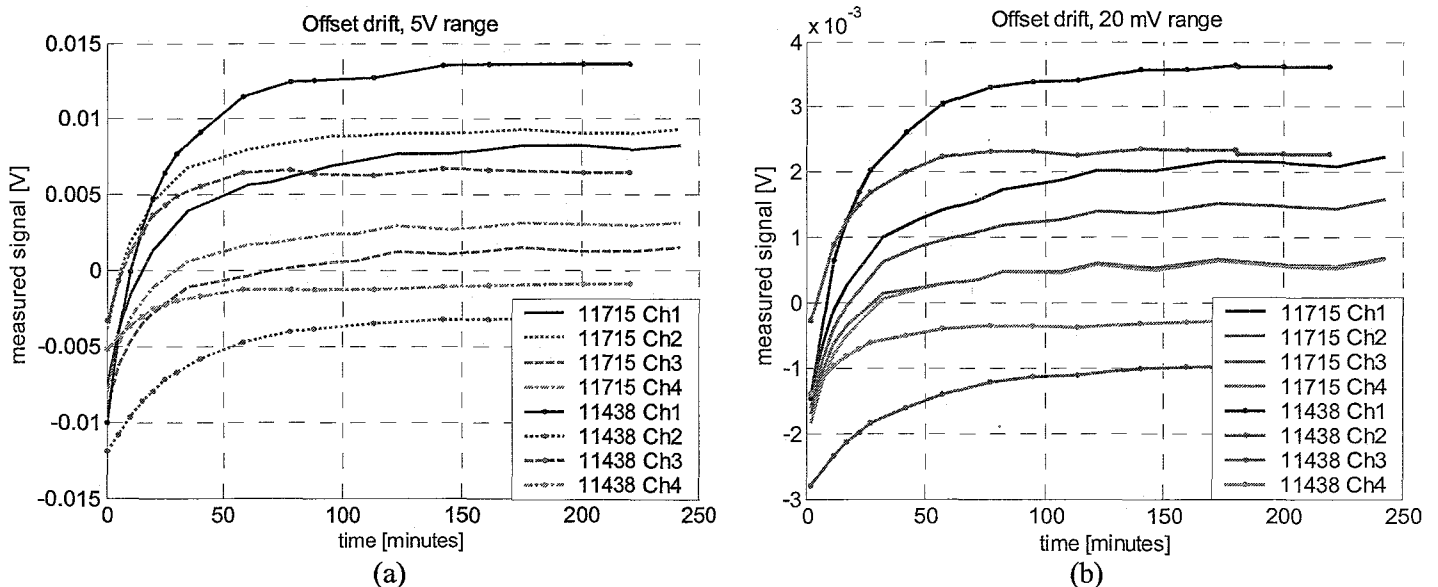
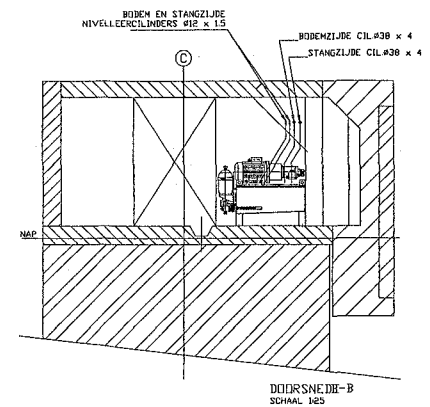
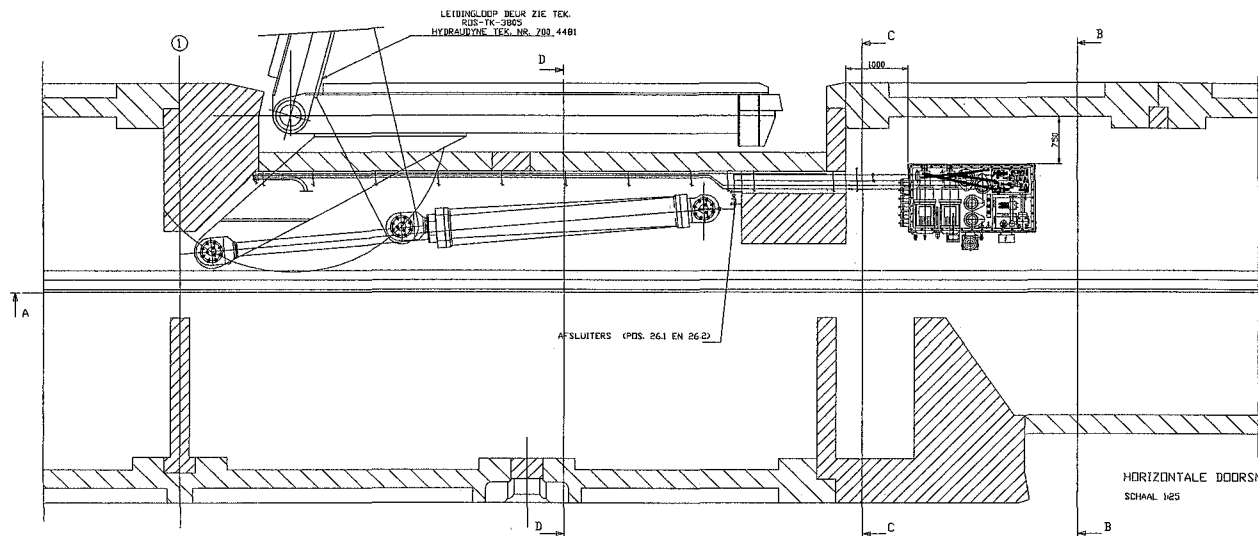


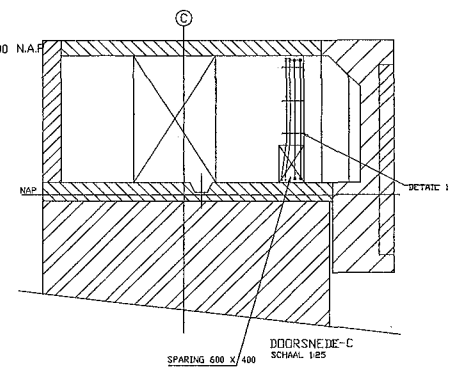
Figure D.4 Time drift of DC-offset in SigLab

(a) 5 V range (b) 20 mV range
59

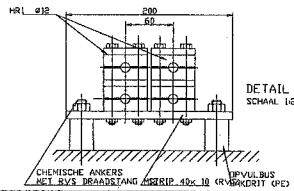
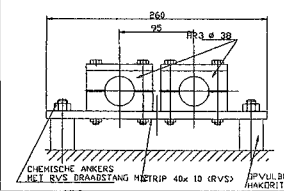
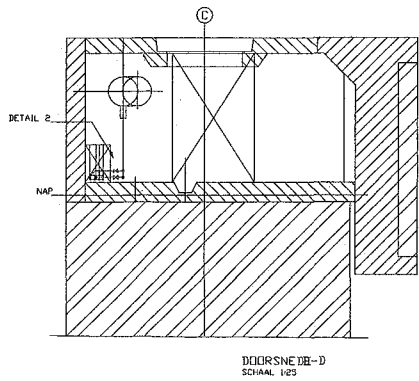
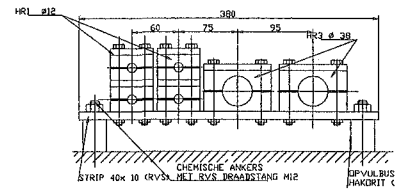
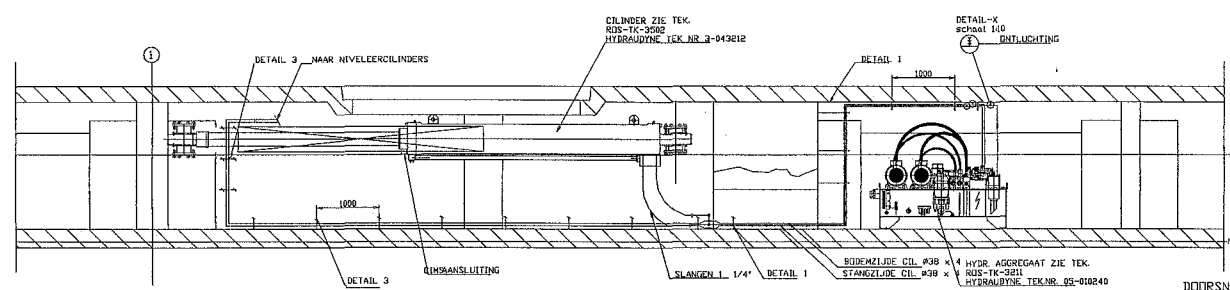
Appendix E Technical drawings



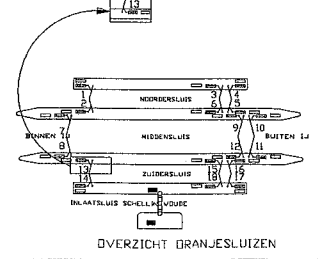
HORizontale DOORSNEDE OP +1.400 NAP
SCHAAFL. 1:25



DOORSNEDE-A
SCHAAFL. 1:25



TEKENING 180° VERDRAAD GETEKEND T.D.V.



AS BUILT

TEKARLENK		MNSA 1998-19979									
LEIDINGLOOP	ZUIDERSLUIS AS - C	1:25	10-10-00								
HYDROGARE		7004517	A0 C								
TEKENING	7004517	TEKNIK	A0 C								
<table border="1"> <tr> <th>NO</th> <th>VERSIJ</th> <th>VERSIJ</th> <th>VERSIJ</th> </tr> <tr> <td>1</td> <td>1</td> <td>1</td> <td>1</td> </tr> </table>				NO	VERSIJ	VERSIJ	VERSIJ	1	1	1	1
NO	VERSIJ	VERSIJ	VERSIJ								
1	1	1	1								
<table border="1"> <tr> <th>NO</th> <th>VERSIJ</th> <th>VERSIJ</th> <th>VERSIJ</th> </tr> <tr> <td>1</td> <td>1</td> <td>1</td> <td>1</td> </tr> </table>				NO	VERSIJ	VERSIJ	VERSIJ	1	1	1	1
NO	VERSIJ	VERSIJ	VERSIJ								
1	1	1	1								
<table border="1"> <tr> <th>NO</th> <th>VERSIJ</th> <th>VERSIJ</th> <th>VERSIJ</th> </tr> <tr> <td>1</td> <td>1</td> <td>1</td> <td>1</td> </tr> </table>				NO	VERSIJ	VERSIJ	VERSIJ	1	1	1	1
NO	VERSIJ	VERSIJ	VERSIJ								
1	1	1	1								

